Nonperturbative electromagnetic lepton-pair production in peripheral relativistic heavy-ion collisions

J. C. Wells
Center for Computationally Intensive Physics, Oak Ridge National Laboratory, Oak Ridge, Tennessee 37831; Physics Division, Oak Ridge National Laboratory, Oak Ridge, Tennessee 37831; and Department of Physics and Astronomy, Vanderbilt University, Nashville, Tennessee 37235

V. E. Oberacker and A. S. Umar
Center for Computationally Intensive Physics, Oak Ridge National Laboratory, Oak Ridge, Tennessee 37831 and Department of Physics and Astronomy, Vanderbilt University, Nashville, Tennessee 37235

C. Bottcher, M. R. Strayer, and J.-S. Wu
Center for Computationally Intensive Physics, Oak Ridge National Laboratory, Oak Ridge, Tennessee 37831 and Physics Division, Oak Ridge National Laboratory, Oak Ridge, Tennessee 37831

G. Plunien
Department of Physics and Astronomy, Vanderbilt University, Nashville, Tennessee 37235
(Received 7 November 1991)

We discuss a nonperturbative treatment of lepton-pair production caused by the strong and sharply pulsed electromagnetic fields generated in peripheral relativistic heavy-ion collisions with an emphasis on the capture process into the atomic K shell. We calculate, in a field-theoretical framework, impact-parameter-dependent probabilities and cross sections for such processes by solving the time-dependent Dirac equation on a three-dimensional Cartesian lattice using the basis-spline collocation method. We give a full discussion of the stationary states used in computing S-matrix elements. Use of the axial gauge for the electromagnetic potentials produces an interaction easier to implement on the lattice than the Lorentz gauge. Preliminary calculations are given for muon-pair production with capture into the K shell in collisions of $^{197}Au+^{197}Au$ at collider energies per nucleon of 2 and 100 GeV.

PACS number(s): 11.80.−m, 13.10.+q, 12.20.−m

I. INTRODUCTION

The prospect of colliding-beam accelerators capable of producing collisions of highly stripped high-Z ions, at fixed-target energies per nucleon up to 20 TeV, has motivated much interest in lepton-pair production from the QED vacuum. The electromagnetic fields involved in such collisions contain large Fourier components which give rise to sizable pair production [1,2]. These collisions provide an opportunity to study nonperturbative QED in an entirely new energy regime. The electromagnetic production of lepton pairs using heavy ions is fundamentally different from the production mechanisms using light particles, since in the former the coupling constant is strongly enhanced, e.g., for very heavy systems (Au+Au,U+U) $Z\alpha \approx 0.6$, where Z is the atomic number of a participant heavy ion and α is the fine-structure constant. Applying perturbation theory to this process at high energies results in probabilities which violate unitarity and cross sections which violate the Froissart bound [3,4]. This evidence, along with nonperturbative model studies, clearly suggests that higher-order QED effects will be important at the relativistic heavy-ion collider (RHIC) [2,5].

In addition to the fundamental questions regarding lepton-pair production and nonperturbative QED, an accurate description of electromangetic lepton-pair production is important for both detector design and collider performance at new experimental facilities such as RHIC. Hadronic lepton-pair production has been widely discussed as a possible tool for probing the formation and the decay of the quark-gluon plasma phase of matter which is to be produced in extremely relativistic heavy-ion collisions [6]. Suggestions by several authors indicate that other sources of lepton pairs might possibly mask the leptonic signals originating from the plasma phase [7–9]. Electromagnetic lepton-pair production caused by highly stripped heavy ions in relativistic motion is estimated to be a major contribution to this physical background [1,2]. In addition, bound-free lepton-pair production in peripheral collisions changes the charge state of a participant heavy ion, leading to a decrease in the luminosity lifetime of the collider [7]. Accurate predictions of the cross sections for this process are important for the new generation of high-energy colliders, as cross sections for electromagnetic lepton-pair production with capture increase with energy.

There is a long history of the use of perturbative

methods in studying the electromagnetic production of lepton pairs, and this topic is recently reviewed in Refs. [10,11]. However, as mentioned above, we plan to study nonperturbative effects in lepton-pair production, since the applicability of perturbation theory is doubtful at high Z and high energy. Recently, coupled channel calculations have been performed at moderately relativistic energies which suggest that perturbative approaches greatly underestimate electron-pair production with capture into the K shell at moderate impact parameters [12].

In this paper, we outline a nonperturbative approach to electromagnetic lepton-pair production, which is applicable over a wide range of relativistic energies. Beginning with the QED Lagrange density, we make reasonable assumptions about the nature of the lepton and radiation fields in peripheral relativistic heavy-ion collisions which simplify the equations of motion to the time-dependent Dirac equation and Maxwell equations. In doing this, we maintain the field-theoretical tools for calculating particle production. We implement the solution of the Dirac equation using the lattice basis-spline collocation method [13,14] in which quantum-state vectors and coordinate-space operators are given by expansions in terms of basis-spline functions and represented on a discrete spatial grid. This method is very efficient and allows us to avoid notorious difficulties such as the fermion-doubling problem and to preserve the basic conservation laws on the lattice [13]. Our preliminary calculations are limited to muon-pair creation with capture into the K shell, neglecting, for now, the more probable and more nonperturbative electron-capture process. We do this because the necessary $1s$ bound state of the target is easier to compute for the muonic atom than for the electronic atom with our lattice methods. In our calculations, we neglect free-pair production, since this process requires the time evolution of many states, whereas the capture process requires the time evolution of only a few states.

In developing our approach to nonpeturbative lepton-pair production, we have performed time-dependent model calculations in one and three spatial dimensions [8,13,15]. In the three-dimensional calculation for the $^{197}\mathrm{Au}+^{197}\mathrm{Au}$ system at collider energies of 0.2, 1.0, and 2.0 GeV per nucleon, we estimated the probabilities for muon-pair production with capture into the K shell to be several orders of magnitude greater than the standard perturbation theory at grazing impact parameters [15]. This work gave the first clear computational indication for the nonperturbative nature of lepton-pair production in relativistic heavy-ion collisions, though it required small lattice sizes and a screened projectile interaction to make the size of the calculation manageable. Here, we improve these three-dimensional calculations by using the physical interaction, i.e., no screening is used. This is made possible by taking advantage of the freedom we have in choosing the gauge for our electromagnetic interaction.

The plan for the paper is as follows. In Sec. II, we derive the equations of motion and impact-parameter-dependent probabilities for the creation of leptons from the vacuum. In Sec. III, we discuss our numerical methods. Section IV describes the electromagnetic interaction and our choice of gauge. The paper concludes with a discussion of our preliminary results for muon-pair production with capture.

II. THEORETICAL FRAMEWORK

Our formalism for nonperturbative lepton-pair production in relativistic heavy-ion collisions can be derived from a semiclassical least-action principle [13]. In the following, we give an alternative derivation related to the approach of Reinhardt and co-workers to e^+e^- production in nonrelativistic heavy-ion reactions [15–17]. The main difference between this present treatment and the derivation involving the semiclassical action is that here we neglect the residual interactions among the leptons at an earlier stage of approximation. Reference [18] gives a similar derivation in first quantization. Throughout this paper, we use natural units, i.e., $\hbar=c=m_0=1$. This implies that energies are measured in units of the lepton rest mass m_0c^2 and length, and time units are the lepton Compton wavelength $\lambda_C=\hbar/m_0c$ and Compton time $\tau_C=\lambda_C/c$, respectively. In general, we denote quantum-field operators by a hat over the mathematical symbol, e.g., $\hat{\psi}$ is the lepton-field operator.

A. Field-theoretical approach

Following the notation in Ref. [19] for the Dirac matrices, we begin with the standard QED Lagrange density operator

$$\mathcal{L}_{\mathrm{QED}}=\hat{\psi}^{\dagger}\gamma^0(\gamma^\mu i\partial_\mu-1)\hat{\psi}-\tfrac{1}{4}\hat{F}_{\mu\nu}\hat{F}^{\mu\nu}-\hat{j}^\mu\hat{A}_\mu\ , \tag{1}$$

where

$$\hat{j}^\mu=\hat{j}^\mu_{\mathrm{lept}}+\hat{j}^\mu_{\mathrm{ext}}=e\hat{\psi}^{\dagger}\gamma^0\gamma^\mu\hat{\psi}+\hat{j}^\mu_{\mathrm{ext}} \tag{2}$$

denotes the total four-current density operator consisting of the lepton current and the conserved, external current generated by the colliding heavy nuclei. The total radiation field $\hat{A}_\mu$ is given by

$$\hat{A}_\mu=\hat{A}^{\mathrm{lept}}_\mu+\hat{A}^{\mathrm{ext}}_\mu+\hat{A}^{\mathrm{free}}_\mu\ , \tag{3}$$

where we imply the obvious decomposition into the contributions $\hat{A}^{\mathrm{lept}}_\mu$ and $\hat{A}^{\mathrm{ext}}_\mu$ generated by the lepton current $\hat{j}^\mu_{\mathrm{lept}}$ and the external current $\hat{j}^\mu_{\mathrm{ext}}$ of the moving heavy ions, respectively. The term $\hat{A}^\mu_{\mathrm{free}}$ denotes the free radiation field. By varying the action integral

$$S_{\mathrm{QED}}=\int d^4x\,\mathcal{L}_{\mathrm{QED}} \tag{4}$$

with respect to the field operators $\hat{\psi}$ and $\hat{A}_\mu$, we obtain the Euler-Lagrange equations of motion for the quantum fields

$$[\gamma^\mu(i\partial_\mu+e\hat{A}_\mu)-1]\hat{\psi}(x)=0\ , \tag{5}$$

$$\partial_\mu\hat{F}^{\mu\nu}(x)=\hat{j}^\nu(x)\ . \tag{6}$$

These equations of motion are difficult to solve and we will make the following simplifying assumptions. First, we choose to neglect the leptonic current $\hat{j}^\mu_{\mathrm{lept}}$ in Eq. (6)

and the corresponding electromagnetic field $\hat{A}_\mu^{\text{lept}}$ in Eq. (5), in comparison to the external current $\hat{j}_{\text{ext}}^\mu$ and the external field $\hat{A}_\mu^{\text{ext}}$, respectively. This decouples the field equations of motion. Neglect of the leptonic current is justified, as it is much smaller than the strong, external heavy-ion current. We also treat the contribution to $\hat{A}_\mu$ from the external heavy ions classically by solving Maxwell's equations, i.e., $\hat{A}_\mu^{\text{ext}} \rightarrow \langle \hat{A}_\mu^{\text{ext}} \rangle_{\text{class}} = A_\mu^{\text{ext}}$. Furthermore, we neglect QED radiative corrections like vacuum polarization and self-energy effects arising from interactions of the lepton field with the free radiation field, i.e., $\hat{A}_\mu^{\text{free}} = 0$. The classical treatment of the radiation field is reasonable since the strength of the external field implies a large number of photons. The problem is thus reduced to the solution of the time-dependent Dirac equation, Eq. (7), for the lepton field $\hat{\psi}$, interacting only with an external, classical four-vector potential A_μ^{ext} determined independently by Maxwell's equations, Eq. (8), i.e.,

$$[\gamma^\mu(i\partial_\mu + eA_\mu^{\text{ext}}) - 1]\hat{\psi}(x) = 0 , \tag{7}$$

$$\partial_\mu F_{\text{ext}}^{\mu\nu}(x) = j_{\text{ext}}^\nu(x) . \tag{8}$$

We study the electromagnetic production of lepton pairs in a reference frame where one of the nuclei, henceforth referred to as the target, is at rest. The target nucleus and the lepton interact via the static Coulomb field A_T^0. The only time-dependent interaction $A_P^\mu(t)$ arises from the classical motion of the projectile. Thus it is natural to recast the Dirac equation (7) into the Schrödinger form

$$[H_F + H_P(t)]\hat{\psi}(\mathbf{r},t) = i\frac{\partial}{\partial t}\hat{\psi}(\mathbf{r},t) , \tag{9}$$

where the static Furry Hamiltonian H_F describing the lepton field in the presence of the strong external Coulomb field of the target nucleus, is given by

$$H_F = -i\boldsymbol{\alpha}\cdot\boldsymbol{\nabla} + \beta - eA_T^0 , \tag{10}$$

and the time-dependent interaction between the lepton field and the projectile is

$$H_P(t) = e\boldsymbol{\alpha}\cdot\mathbf{A}_P(t) - eA_P^0(t) , \tag{11}$$

where $\beta \equiv \gamma^0$ and $\boldsymbol{\alpha} \equiv \gamma^0\boldsymbol{\gamma}$. In this way, binding-energy effects to all orders in the coupling constant are taken into account.

Following the usual practice, we expand the lepton-field operator, defined in Eq. (9), in a complete, orthonormal set of single-particle basis states. First, we consider expanding $\hat{\psi}(\mathbf{r},t)$ in the Furry basis $\{\chi_i(\mathbf{r})\}$, i.e., the stationary eigenstates of the Furry Hamiltonian H_F defined in Eq. (10), given by

$$H_F\chi_k(\mathbf{r}) = E_k\chi_k(\mathbf{r}) , \tag{12}$$

which are also proper in and out states for asymptotic times $|t| \rightarrow \infty$, where the interaction $H_P(t)$ is zero. The index k represents the complete set of quantum numbers for the single-particle state $\chi_k(\mathbf{r})$. Such an expansion gives

$$\hat{\psi}(\mathbf{r},t) = \sum_k \hat{a}_k(t)\chi_k(\mathbf{r})\exp(-iE_k t) , \tag{13}$$

where the $\hat{a}_k$'s are operator-valued expansion coefficients. From the anticommutation relations for the fermion field operators $\hat{\psi}$ and $\hat{\psi}^\dagger$, one readily shows that $\hat{a}_k^\dagger$ and $\hat{a}_k$, respectively, describe the creation and annihilation of leptons in state k in the static Coulomb field of the target nucleus. They define what one may call the mathematical vacuum $|0\rangle$ by $\hat{a}_i|0\rangle = 0$, i.e., the state without particles of any kind. We also consider the time-dependent basis of solutions to the full Dirac Hamiltonian $H_F + H_P(t)$,

$$[H_F + H_P(t)]\phi_j(\mathbf{r},t) = i\frac{\partial}{\partial t}\phi_j(\mathbf{r},t) . \tag{14}$$

Expanding $\hat{\psi}$ in this basis results in

$$\hat{\psi}(\mathbf{r},t) = \sum_j \hat{\alpha}_j\phi_j(\mathbf{r},t) , \tag{15}$$

where the operator-valued expansion coefficients $\hat{\alpha}_j$ are quasiparticle destruction operators. In the time-dependent basis $\{\phi_j(\mathbf{r},t)\}$, the states are not stationary and, in general, are linear combinations of the eigenfunctions of the Furry Hamiltonian. Under the influence of the interaction Hamiltonian $H_P(t)$, the single-particle states $\chi_j(\mathbf{r})$ defined in Eq. (12) evolve into the time-dependent states $\phi_j(\mathbf{r},t)$ according to the time-dependent Dirac equation (14). Therefore the index j does not refer to a set of good quantum numbers for $\phi_j(\mathbf{r},t)$, but refers to the quantum numbers of the particular Furry state $\chi_j(\mathbf{r})$ that satisfies the $t \rightarrow -\infty$ boundary condition

$$\lim_{t\rightarrow-\infty}\phi_j(\mathbf{r},t) \rightarrow \chi_j(\mathbf{r})\exp(-iE_j t) . \tag{16}$$

The QED ground state $|\Phi_0\rangle$ in the presence of the undercritical (i.e., $Z_T\alpha < 1$), external field of the target nucleus is a many-lepton state of time-independent one-particle solutions of the Furry Hamiltonian where all states with energies less than $-m_0c^2$ are occupied, i.e., a single Slater determinant of the form

$$|\Phi_0(t\rightarrow-\infty)\rangle \equiv |\Phi_0\rangle = \prod_{i<F}(\hat{a}_i^\dagger)|0\rangle , \tag{17}$$

where $i < F$ denotes states below the Fermi energy $E_F = -m_0c^2$. We have omitted the spatial coordinates for simplicity. The time-evolved QED ground state is

$$\begin{aligned} &|\Phi_0(t)\rangle = \hat{U}(t,t_0\rightarrow-\infty)|\Phi_0\rangle , \\ &\hat{U}^\dagger(t,t_0)\hat{U}(t,t_0) = 1 , \end{aligned} \tag{18}$$

where $\hat{U}(t,t_0)$ is the time-evolution operator defined in the Schrödinger picture by

$$\hat{U}(t,t_0) = \mathcal{T}\exp\left[-i\int_{t_0}^{t} dt'[H_F + H_P(t')]\right] . \tag{19}$$

The quantity $\mathcal{T}$ denotes time-ordering which is necessary in the general case.

Equations (13), (15), and (17) are consistent with the particle-hole (Dirac sea) picture with both positive- and negative-energy states. In order to work in the space-

time picture with physical particles and antiparticles, we now define antilepton creation and annihilation operators with respect to the QED ground state $|\Phi_0\rangle$ via

$$\hat{b}_i \equiv \hat{a}_i^\dagger \ , \quad \hat{b}_i^\dagger \equiv \hat{a}_i \ , \quad i < F \ . \tag{20}$$

These new operators describe creation and annihilation of antiparticles in the static Coulomb field of the target nucleus. Also, the QED ground state is the Furry-vacuum state for the creation of physical particles and antiparticles

$$\begin{aligned} &\hat{a}_p^\dagger|\Phi_0\rangle = |\chi_p^{(+)}\rangle \ , \quad \hat{a}_p|\Phi_0\rangle = 0 \ , \quad p > F \\ &\hat{b}_q^\dagger|\Phi_0\rangle = |\chi_q^{(-)}\rangle \ , \quad \hat{b}_q|\Phi_0\rangle = 0 \ , \quad q < F \ , \end{aligned} \tag{21}$$

where $|\chi_p^{(+)}\rangle$ and $|\chi_p^{(-)}\rangle$ are particle and antiparticle Furry states, respectively. Inserting the canonical transformation Eq. (20), the lepton field operator of Eq. (13) may be written in the form

$$\begin{aligned} \hat{\psi}(\mathbf{r},t) = &\sum_{r<F} \hat{b}_r^\dagger(t)\chi_r^{(-)}(\mathbf{r})\exp(-iE_r t) \\ &+ \sum_{s>F} \hat{a}_s(t)\chi_s^{(+)}(\mathbf{r})\exp(-iE_s t) \ . \end{aligned} \tag{22}$$

In analogy with Eq. (20), we define a new set of quasiparticle creation operators with respect to the time-evolved Furry vacuum $|\Phi_0(t)\rangle$

$$\hat{\beta}_i \equiv \hat{\alpha}_i^\dagger \ , \quad \hat{\beta}_i^\dagger \equiv \hat{\alpha}_i \ , \quad i < F \ . \tag{23}$$

The expansion of the lepton field operator expressed in this new set of operators is

$$\hat{\psi}(\mathbf{r},t) = \sum_{r<F} \hat{\beta}_r^\dagger \phi_r^{(-)}(\mathbf{r},t) + \sum_{s>F} \hat{\alpha}_s \phi_s^{(+)}(\mathbf{r},t) \ . \tag{24}$$

We emphasize that the operators $\hat{\alpha}_j$, $\hat{\alpha}_j^\dagger$, $\hat{\beta}_j$, and $\hat{\beta}_j^\dagger$, defined with respect to the time-evolved vacuum, do not correspond to observable particle or antiparticle states, but are mathematically convenient because they can act directly on the time-evolved (or quasiparticle) vacuum. Knowing the properties of the time-evolution operator and how it acts on the Furry states, Eq. (21), we obtain

$$\begin{aligned} &\hat{\alpha}_p^\dagger|\Phi_0(t)\rangle = |\phi_p^{(+)}(t)\rangle \ , \quad \hat{\alpha}_p|\Phi_0(t)\rangle = 0 \ , \quad p > F \\ &\hat{\beta}_q^\dagger|\Phi_0(t)\rangle = |\phi_q^{(-)}(t)\rangle \ , \quad \hat{\beta}_i|\Phi_0(t)\rangle = 0 \ , \quad q < F \ , \end{aligned} \tag{25}$$

where $|\phi^{(\pm)}(t)\rangle$ are the single-particle solutions of the time-dependent Dirac equation, Eq. (14). The fermion anticommutation relations are preserved for the $\hat{\alpha}$'s and $\hat{\beta}$'s.

Equating the two representations of the field operator, Eqs. (22) and (24), we establish the following transformation between the static and time-dependent representations of the Fock space operators

$$\begin{aligned} \hat{a}_p(t) = &\sum_{s>F} \hat{\alpha}_s \langle \chi_p^{(+)}|\phi_s^{(+)}(t)\rangle \exp(iE_p t) \\ &+ \sum_{r<F} \hat{\beta}_r^\dagger \langle \chi_p^{(+)}|\phi_r^{(-)}(t)\rangle \exp(iE_p t) \ , \quad p > F \end{aligned} \tag{26}$$

$$\begin{aligned} \hat{b}_q^\dagger(t) = &\sum_{s>F} \hat{\alpha}_s \langle \chi_q^{(-)}|\phi_s^{(+)}(t)\rangle \exp(iE_q t) \\ &+ \sum_{r<F} \hat{\beta}_r^\dagger \langle \chi_q^{(-)}|\phi_r^{(-)}(t)\rangle \exp(iE_q t) \ , \quad q < F \ . \end{aligned} \tag{27}$$

B. Observables

After obtaining all the necessary field-theoretical tools, we now evaluate probabilities for lepton-pair production. First, we calculate the expectation values of lepton number operators. Using Eqs. (25), (26), and the anticommutation relations for the $\hat{\alpha}$'s, the inclusive number of leptons created in state $p > F$ is

$$\begin{aligned} \langle \hat{n}_p(t)\rangle &= \langle \Phi_0(t)|\hat{a}_p^\dagger(t)\hat{a}_p(t)|\Phi_0(t)\rangle \\ &= \sum_{r<F} |\langle \chi_p^{(+)}|\phi_r^{(-)}(t)\rangle|^2 \ , \quad p > F \ . \end{aligned} \tag{28}$$

Likewise, using Eqs. (25), (27), and the anticommutation relation for the $\hat{\beta}$'s, the inclusive number of antileptons created in state $q < F$ is

$$\begin{aligned} \langle \hat{\bar{n}}_q(t)\rangle &= \langle \Phi_0(t)|\hat{b}_q^\dagger(t)\hat{b}_q(t)|\Phi_0(t)\rangle \\ &= \sum_{s>F} |\langle \chi_q^{(-)}|\phi_s^{(+)}(t)\rangle|^2 \ , \quad q < F \ . \end{aligned} \tag{29}$$

We evaluate the expectation value of a product of number operators using the anticommutation relations, as well as Eqs. (25)–(27) and the completeness relations for the $\{|\phi_q(t)\rangle\}$ to find the number of correlated particle-antiparticle pairs created,

$$\begin{aligned} \langle \hat{\bar{n}}_q(t)\hat{n}_p(t)\rangle = &\langle \bar{n}_q(t)\rangle\langle n_p(t)\rangle \\ &+ \left| \sum_{r<F} \langle \chi_q^{(-)}|\phi_r^{(-)}(t)\rangle\langle \phi_r^{(-)}(t)|\chi_p^{(+)}\rangle \right|^2 , \\ &q < F, \ p > F \ . \end{aligned} \tag{30}$$

The first term in Eq. (30) describes statistical coincidences, while the second contains coherent correlation effects. Equation (30) holds also in the case of particle-particle and antiparticle-antiparticle correlations if the plus sign is replaced by a minus. One obtains the total inclusive number of leptons and antileptons created by summing over the lepton states in Eq. (28) and the antilepton states in Eq. (29), respectively,

$$N(t) = \sum_{p>F} \sum_{r<F} |\langle \chi_p^{(+)}|\phi_r^{(-)}(t)\rangle|^2 \ , \tag{31}$$

$$\bar{N}(t) = \sum_{q<F} \sum_{s>F} |\langle \chi_q^{(-)}|\phi_s^{(+)}(t)\rangle|^2 \ . \tag{32}$$

The total number of leptons and antileptons must be equal because of charge conservation. One can demonstrate this identity explicitly in two ways. The first and most direct way is to use the completeness relations for the sets of basis states $\{|\phi_r\rangle\}$ and $\{|\chi_p\rangle\}$. Alternatively, one may exploit the transformation properties of the time-evolution operator and the Dirac spinors under time reversal to show the equality of the total number of leptons and antileptons produced.

Since the expectation value $\langle \hat{n}_p(+\infty)\rangle$ in Eq. (28) is

positive definite and normalized to unity as a consequence of the Pauli principle and the unitarity of the time-evolution operator, it is interpreted as the probability P_p that a lepton will be created in state $p > F$ regardless of what happens to the associated antilepton. Likewise, $P_q = \langle \hat{\bar{n}}_q(+\infty) \rangle$ is the corresponding inclusive probability for an antilepton to be created in state $q < F$. The number of correlated particle-antiparticle paris produced in individual states, Eq. (30), also has correct normalization to be interpreted as a probability, e.g., $P_{q,p} = \langle \hat{\bar{n}}_q(+\infty) \hat{n}_p(+\infty) \rangle$ for $q < F$ and $p > F$.

In many experimental situations, the quantity of interest is the probability for producing a lepton of a specific energy regardless of its angular momentum. Calculating this requires the averaging of the probabilities for all leptons produced with a specified energy. However, if one is interested in pair production with capture, or if the continuum is discretized on a lattice, there will be no need for such averaging over the magnitude of the total angular momentum j_p because of the discrete nature of the spectrum. Only averaging over the projection of the total angular momentum μ_p is required, e.g., the probability of creating a lepton with energy E_p is

$$P_{E_p} = \frac{1}{2\mu_p + 1} \sum_{\mu_p = -j_p}^{+j_p} P_p = \frac{1}{2\mu_p + 1} \sum_{\mu_p = -j_p}^{+j_p} \langle \hat{n}_p(+\infty) \rangle \ . \tag{33}$$

From Eqs. (28)–(32) we see that to compute probabilities for lepton-pair production, we must first project time-evolved single-particle states onto static Furry states, i.e., compute single-particle transition amplitudes. Measurable probabilities are the squares of the asymptotic ($t \to \infty$) limit of these transition amplitudes. With this in mind, we identify these asymptotic transition amplitudes with matrix elements of the scattering operator, defined as $\hat{S} \equiv \hat{U}(+\infty, -\infty)$, in the Furry basis

$$\langle \chi_j | \hat{S} | \chi_i \rangle = S_{i \to j} = \langle \chi_j | \phi_i(\infty) \rangle \ . \tag{34}$$

One may use the time-reversal symmetry of the Dirac equation to reduce the effort needed to compute some observables by applying the principle of semidetailed balance [20]

$$\sum_{\mu_a = -j_a}^{j_a} \sum_{\mu_b = -j_b}^{j_b} |S_{a \to b}| = \sum_{\mu_a = -j_a}^{j_a} \sum_{\mu_b = -j_b}^{j_b} |S_{b \to a}| \ . \tag{35}$$

For example, consider the probability for lepton-pair production with capture into a bound state of the target. Rewriting Eq. (33), using Eqs. (28) and (34), we obtain

$$P_{E_p} = \frac{1}{2\mu_p + 1} \sum_{\mu_p = -j_p}^{+j_p} \sum_{r < F} |S_{r \to p}|^2 \ , \tag{36}$$

where p is the bound state. To compute Eq. (36), we must time evolve all the negative-energy continuum states $|\chi_r^{(-)}\rangle$ and project these onto the bound state $|\chi_p^{(+)}\rangle$. Using Eq. (35), we obtain instead an expression where only $2j_p + 1$ time-dependent solutions of the Dirac equation are required,

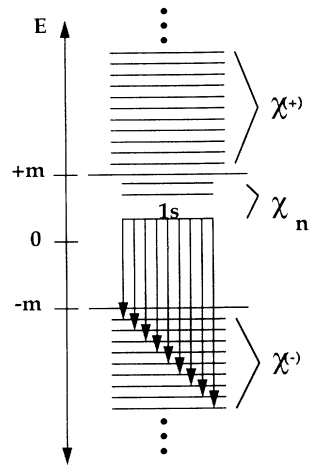

FIG. 1. Depicted is the stationary Furry spectrum consisting of bound states (χ_n), positive ($\chi^{(+)}$), and negative-energy ($\chi^{(-)}$) continuum states. Equation (37) is illustrated by showing transitions of the $1s$ state to the negative-energy continuum.

$$P_{E_p} = \frac{1}{2\mu_p + 1} \sum_{\mu_p = -j_p}^{+j_p} \sum_{r < F} |S_{p \to r}|^2 \ , \quad p > F \ . \tag{37}$$

Thus, for computational purposes, we view lepton-pair production from the QED vacuum with K-shell capture as an ionization process of a bound lepton in the $1s$ state to unoccupied negative-energy continuum states. We illustrate the probability defined by Eq. (37) in Fig. 1 by showing transitions from the $1s$ state to the discretized negative-energy continuum. This application of semidetailed balance has been used extensively in similar calculations [16–18,21]. In the case of K-shell capture, one needs to compute only two time-dependent Dirac states $|\phi_{1s}^{\mu_p = \pm 1/2}(t)\rangle$. Currently, we are forced to assume that both magnetic substates contribute equally to $P_{E_{1s}}$, as our method chosen to compute static bound states is unable to distinguish eigenvectors of degenerate eigenvalues.

III. NUMERICAL IMPLEMENTATION

In the course of Sec. II, we reduced the problem of electromagnetic lepton-pair production in relativistic heavy-ion collisions to that of computing single-particle S-matrix elements in the Furry basis. We perform all calculations using a lattice approach through which we obtain a discrete representation of all Dirac spinors and coordinate-space operators on a three-dimensional Cartesian mesh. The use of Cartesian coordinates avoids the disadvantages of rotating frames and the complicated metrics of spherical coordinate systems. The time-dependent electromagnetic fields exhibit no usable symmetry in any case. We implement our lattice solution using the basis-spline collocation method which is discussed in detail in Refs. [13,14]. In Sec. III A, we give a basic introduction to the basis-spline collocation method by obtaining a lattice representation of the Furry Hamiltonian,

Eq. (12), in three Cartesian dimensions. We limit this discussion and our current calculations to the special case of lattices inside cubic boxes with uniform spacing in all three directions. However, the basis-spline collocation method is well studied for nonuniform lattice spacing. To construct the necessary S-matrix elements, we must compute the stationary states of the Furry Hamiltonian and then evolve these states in time. We discuss these issues in Secs. III B and III C.

A. Lattice basis-spline collocation method

Splines of order M are functions $S^M(x)$ of a single real variable belonging to the class $\mathcal{C}^{(M-2)}$ with continuous $(M-2)$th derivatives. These functions are piecewise continuous, as they are constructed from continuous polynomials of $(M-1)$th order joined at points in an ordered set $\{x_i\}$ called knots. Basis splines are splines with minimal support, i.e., they are zero outside the range of $M+1$ consecutive knots $x_i, x_{i+1}, \ldots, x_{i+M}$, and are positive definite. We label these functions with the index of their first knot $B_i^M(x)$. The explicit construction of basis-spline functions is explained in Ref. [14]; however, we show a fifth-order example in Fig. 2.

Consider a region of space with boundaries at $x_{\min}$ and $x_{\max}$ and containing $N+1$ knots, including the knots on the boundaries. For a set of Mth-order basis splines to be complete, M of the functions must be nonzero on each knot interval $x_i \rightarrow x_{i+1}$ within the physical region. For this to occur, $M-1$ basis splines must extend outside each boundary. Therefore we require a knot sequence from x_1 to x_{N+2M-1} in order to construct a complete set of functions, where x_M and x_{M+N} correspond to the lower and upper physical boundaries, respectively. The basis splines for the region are naturally numbered as $B_1^M(x), B_2^M(x), \ldots, B_{N+M-1}^M(x)$, as shown in the example given in Fig. 3.

We generalize the procedure given above to construct a complete set of functions in a three-dimensional region by expanding in terms of products of basis-spline functions, i.e., $B_i^M(x)B_j^M(y)B_k^M(z)$. We expand each of the four Dirac spinor components, denoted by the index p, in such a basis (using covariant notation),

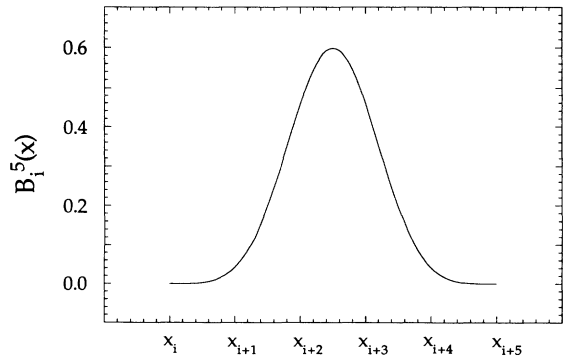

FIG. 2. Depicted is a fifth-order basis-spline function $B_i^5(x)$, which is constructed from continuous fourth-order polynomials connected at the knots, $x_i, \ldots, x_{i+5}$.

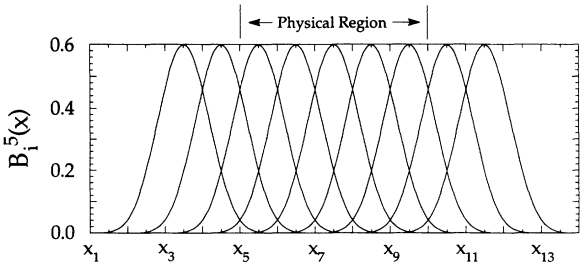

FIG. 3. Depicted is a complete set of fifth-order basis-spline functions for the region $x_5 \le x \le x_{10}$ for homogeneous lattice spacing. The functions are labeled from the left as $B_1^5(x), B_2^5(x), \ldots, B_9^5(x)$. The knot sequence is $x_1, x_2, \ldots, x_{14}$, and the collocation points for this region are placed at $x_\alpha = (x_{\alpha+4} + x_{\alpha+5})/2$ for $\alpha = 1, \ldots, 5$.

$$\chi^{(p)}(x,y,z) = \sum_{i,j,k=1}^{N+M-1} B_i^M(x)B_j^M(y)B_k^M(z)c_{(p)}^{ijk} , \quad p = 1, \ldots, 4 , \tag{38}$$

where we suppress quantum-number indices for clarity and $c_{(p)}^{ijk}$ denotes the complex expansion coefficients for the pth component of the spinor. All state functions in this paper are determined with periodic boundary condition which are easily imposed by renumbering $B_{N+1}^M, \ldots, B_{N+M-1}^M$ as $B_1^M, \ldots, B_{M-1}^M$, respectively, without changing their location. Consequently, the basis-spline index i will run to N instead of $N+M-1$. The details of implementing nonperiodic boundary conditions are discussed in Ref. [14].

We forsake the continuous description of the Dirac spinor for a lattice representation of $\chi(\mathbf{r})$ through the collocation method, in which the spinor is known only at each of the collocation points $(x_\alpha, y_\beta, z_\gamma)$, which define the lattice, i.e., $\chi(\mathbf{r}) \rightarrow \chi_{\alpha,\beta,\gamma}$. Using an underline to denote vectors and matrices in collocation space, the Dirac spinor $\underline{\chi}$ will be a column vector of $N^3 \times 4$ complex numbers. To implement the lattice description of the Dirac spinor using the basis-spline expansion, we create a linear system of equations by evaluating Eq. (38) at the collocation points

$$\chi_{\alpha\beta\gamma}^{(p)} = \sum_{i,j,k=1}^{N} B_{\alpha i}B_{\beta j}B_{\gamma k}c_{(p)}^{ijk} , \quad p = 1, \ldots, 4 \tag{39}$$

where $B_{\alpha i} \equiv B_i^M(x_\alpha)$; the order M is omitted for simplicity. There are a number of ways to choose collocation points. An optimal and simple choice when using odd-order basis-splines is to place one collocation point at the center of each equally spaced knot interval within the physical boundaries,

$$x_\alpha = \frac{x_{\alpha+M-1} + x_{\alpha+M}}{2} , \quad \alpha = 1, \ldots, N . \tag{40}$$

The collocation points are denoted by Greek indices.

The essence of the lattice approach is to eliminate the expansion coefficients $c_{(p)}^{ijk}$ from the set of equations in Eq. (39) using the inverse of the matrices $B_{\alpha j}, B_{\beta j}$, and $B_{\gamma k}$,

$$c^{ijk}_{(p)} = \sum_{\alpha,\beta,\gamma=1}^{N} B^{i\alpha}B^{j\beta}B^{k\gamma}\chi^{(p)}_{\alpha\beta\gamma} , \tag{41}$$

where the inverse matrix, denoted $B^{i\alpha} \equiv [B^{-1}]_{i\alpha}$, plays the role of a metric in the discrete collocation space. The choice of the collocation points given above in Eq. (40) ensures that the matrix $B_{i\alpha}$ is nonsingular.

We now discuss the collocation-lattice representation of a linear, coordinate-space operator $\mathcal{O}$ by considering its action on the basis-spline expansion of $\chi(\mathbf{r})$ in Eq. (38),

$$\mathcal{O}\chi^{(p)}(x,y,z) = \sum_{i,j,k=1}^{N} [\mathcal{O}B^M_i(x)B^M_j(y)B^M_k(z)]c^{ijk}_{(p)} . \tag{42}$$

As before, we create a system of equations by evaluating Eq. (42) at the collocation points,

$$[\mathcal{O}\chi^{(p)}]_{\alpha\beta\gamma} = \sum_{i,j,k=1}^{N} [\mathcal{O}B^M_i(x)B^M_j(y)B^M_k(z)]_{x_\alpha y_\beta z_\gamma} c^{ijk}_{(p)} . \tag{43}$$

We now eliminate the expansion coefficients $c^{ijk}_{(p)}$ from Eq. (43) using Eq. (41) to obtain

$$[\mathcal{O}\chi^{(p)}]_{\alpha\beta\gamma} = \sum_{\mu,\nu,\xi=1}^{N} O^{\mu\nu\xi}_{\alpha\beta\gamma}\chi^{(p)}_{\mu\nu\xi} , \tag{44}$$

where we define the lattice representation of the coordinate-space operator as

$$O^{\mu\nu\xi}_{\alpha\beta\gamma} \equiv \sum_{i,j,k=1}^{N} [\mathcal{O}B^M_i(x)B^M_j(y)B^M_k(z)]_{x_\alpha, y_\beta, z_\gamma} B^{i\mu}B^{j\nu}B^{k\xi} . \tag{45}$$

Consider the collocation lattice representation of the gradient operator in Cartesian coordinates. Using Eq. (45), its lattice representation is

$$D^{\mu\nu\xi}_{\alpha\beta\gamma} = e_1 \sum_{i=1}^{N} B'_{\alpha i}B^{i\mu}\delta^\nu_\beta\delta^\xi_\gamma + e_2 \sum_{j=1}^{N} B'_{\beta j}B^{j\nu}\delta^\mu_\alpha\delta^\xi_\gamma + e_3 \sum_{k=1}^{N} B'_{\gamma k}B^{k\xi}\delta^\mu_\alpha\delta^\nu_\beta , \tag{46}$$

where $B'_{\alpha i} = dB_i(x)/dx|_{x_\alpha}$ and e_j is a unit vector in the jth coordinate direction. In matrix notation, we denote Eq. (46) as

$$\underline{\mathbf{D}} = e_1\underline{D}_1 + e_2\underline{D}_2 + e_3\underline{D}_3 , \tag{47}$$

with the obvious definition of the matrices $\underline{D}_1$, $\underline{D}_2$, and $\underline{D}_3$. Using Eq. (47), the lattice representation of the Dirac equation with the Furry Hamiltonian, Eq. (12), may be written

$$\underline{H}_F\underline{\chi} = E\underline{\chi} , \tag{48}$$

where

$$\underline{H}_F = -i\boldsymbol{\alpha}\cdot\underline{\mathbf{D}} + \beta - e\underline{A}^0_T . \tag{49}$$

Notice that local operators like the target's interaction with the lepton $\underline{A}^0_T$ are diagonal matrices of their values at the collocation points.

In summary, the collocation points define a lattice on which the calculations are performed; neither the splines or the knots appear explicitly again once the lattice representation of the operators has been obtained at the beginning of the calculation. We have reduced the partial differential equation Eq. (12) to a series of linear algebraic equations which may be solved using iterative techniques. As a consequence of eliminating the expansion coefficients from the theory, $\underline{H}_F$ has a blocked, nonsparse representation which is self-adjoint for periodic boundary conditions.

B. Fermion-doubling problem

The lattice representation of H_F, given in Eq. (49), is unsuitable for our purposes, as it exhibits the fermion-doubling problem. This difficulty is present in all transcriptions of the Dirac equation to the lattice using a symmetric representation of the first derivative operator and results in 2^d times the number of fermionic stationary states, where d is the number of dimensions of space-time involved in the lattice formulation [22]. In dynamical problems, fermion doubling causes high-momentum components, which grow exponentially, to appear in the wave function at random [13]. Different authors discuss the causes of the spectral doubling in terms of the nontrivial topology of the lattice momentum space [22–25], (i.e., the lattice imposes a maximum momentum on the lattice states), the topology of the lattice coordinate space [26], or the difficulties associated with the chiral anomaly of fermionic quantum field theories [23,25]. In general, it seems impossible to write a lattice Dirac equation in more than 1+1 dimensions yielding the correct fermion spectrum, involving only local couplings, and admitting a continuous global chiral invariance in the massless limit [26].

References [13,26,27] give a prescription for overcoming the fermion-doubling problem for the special case of a one-dimensional Dirac equation on a lattice. As this example illustrates the nature of the fermion doubling and serves as the basis for our strategy in attacking the pathology with the basis-spline collocation method in three dimensions, consider the stationary states of the free Dirac equation,

$$h_D\psi(x) = E\psi(x) . \tag{50}$$

In one dimension, the Dirac Hamiltonian is independent of spin and it suffices to specify h_D in a two-component representation as

$$h_D = \begin{bmatrix} +1 & -i\partial_x \\ -i\partial_x & -1 \end{bmatrix} . \tag{51}$$

The state ψ is a two component spinor

$$\psi = \begin{bmatrix} G \\ F \end{bmatrix} , \tag{52}$$

where G and F denote the upper and lower components of ψ, respectively. Therefore our problem is to solve two first-order coupled differential equations

$$G'(x)=i(E+1)F(x)\ ,\quad F'(x)=i(E-1)G(x)\ . \tag{53}$$

Consider first implementing the solution of Eqs. (53) by discretizing the eigenstates of Eq. (50) on a simple finite difference lattice $x_j=j\Delta x$, $1\le j\le N$, using a symmetric representation of the derivative operator,

$$G_j'=(G_{j+1}-G_{j-1})/2\Delta x\ . \tag{54}$$

With this approach, Eqs. (53) may be combined into the difference formula

$$G_{j+2}+G_{j-2}-2G_j=(2\Delta x)^2(1-E^2)G_j\ . \tag{55}$$

A solution of this equation having periodic boundary conditions is given by

$$G_j=g_0\exp(ikx_j)\ ,\quad k=2\pi\eta/(N-1)\ , \tag{56}$$

with η taking on the values $\pm1,\pm2,\ldots,\pm(N-1)/2$. The energy eigenvalues of these solutions obey the dispersion relation,

$$E_k^2=1+\frac{k_0^2}{\pi^2}\sin^2\left[\frac{\pi k}{k_0}\right]\ , \tag{57}$$

where $k_0=\pi/\Delta x$ is the maximum momentum allowed on the lattice. This spectrum Eq. (57) is compared in Fig. 4 to the usual continuum result $E^2=1+k^2$. The energies of the states on the lattice with small momenta $k/k_0\le\frac{1}{5}$ are in good agreement with the exact results. However, for larger values of the momenta, marked deviations appear, and for $k/k_0\ge\frac{1}{2}$ and above, the lattice spectrum develops an unphysical second branch having characteristically low-energy eigenvalues associated with large momenta.

Alternatively, consider using the elementary forward- and backward-difference formulas to discretize the lower and upper components of the Dirac spinor, respectively,

$$\begin{aligned}&G_j-G_{j-1}=i\Delta x(E+1)F_j\ ,\\&F_{j+1}-F_j=i\Delta x(E-1)G_j\ .\end{aligned} \tag{58}$$

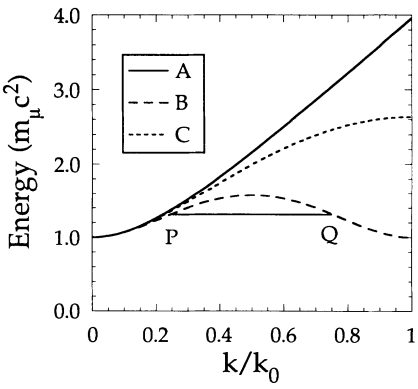

FIG. 4. Fermion doubling is illustrated by plotting the energy vs momentum in units of $k_0=\pi/\Delta x$ for the stationary states of the free Dirac equation in one dimension, where Δx is the lattice spacing: *A*, the exact relation; *B*, Eq. (57); *P* and *Q* label two momentum solutions with the same energy; *C*, Eq. (60), showing a single-valued, finite-difference dispersion relation.

Using Eqs. (58), Eqs. (53) may be combined to form the difference formula

$$G_{j+2}+G_{j-2}-2G_j=(\Delta x)^2(1-E^2)G_j\ . \tag{59}$$

With the periodic solutions in Eq. (56), this difference equation yields the modified dispersion relation,

$$E_k^2=1+\frac{4k_0^2}{\pi^2}\sin^2\left[\frac{\pi k}{2k_0}\right]\ , \tag{60}$$

which, as shown in Fig. 4, does not exhibit the doubled spectrum.

We generalize the idea of employing forward- and backward-difference formulas in representing the derivative operator to the more complex three-dimensional basis-spline collocation method as follows. We first use Eq. (45) to obtain a lattice representation of the Laplacian operator in Cartesian coordinates,

$$\begin{aligned}\Delta_{\alpha\beta\gamma}^{\mu\nu\xi}=&\sum_{i=1}^{N}B''_{\alpha i}B^{i\mu}\delta_\beta^\nu\delta_\gamma^\xi+\sum_{j=1}^{N}B''_{\beta j}B^{j\nu}\delta_\alpha^\mu\delta_\gamma^\xi\\&+\sum_{k=1}^{N}B''_{\gamma k}B^{k\xi}\delta_\alpha^\mu\delta_\beta^\nu\ ,\end{aligned} \tag{61}$$

or in matrix notation

$$\underline{\Delta}=\underline{\Delta}_1+\underline{\Delta}_2+\underline{\Delta}_3\ . \tag{62}$$

We factorize each $\underline{\Delta}_i$ into a lower- and upper-triangular form by Cholesky decomposition, $\underline{\Delta}_i=\underline{D}_i^-\underline{D}_i^+$, in analogy to backward and forward finite-difference formulas. These $\underline{D}^\pm$ matrices are uniquely specified by the condition $D_\alpha^{\alpha-}=|D_\alpha^{\alpha+}|$. We implement the $\underline{D}_i^+$ and $\underline{D}_i^-$ as the lattice representation of the first derivative operator for the lower and upper components of the Dirac spinor, respectively,

$$\underline{H}_F=\begin{bmatrix}\underline{1}-e\underline{A}_T^0 & -i\boldsymbol{\sigma}\cdot\underline{\mathbf{D}}^+\\ -i\boldsymbol{\sigma}\cdot\underline{\mathbf{D}}^- & -\underline{1}-e\underline{A}_T^0\end{bmatrix}\ , \tag{63}$$

where $\underline{\mathbf{D}}^\pm=e_1\underline{D}_1^\pm+e_2\underline{D}_2^\pm+e_3\underline{D}_3^\pm$. This prescription succeeds in avoiding spectral doubling while preserving the hermiticity of the lattice Furry Hamiltonian and simple conservation laws on the lattice [13]. It does not admit continuous chiral invariance, which however, is not important for our application.

C. Computation of stationary states

The complete eigensolution of $\underline{H}_F$, providing its full spectrum of stationary states, currently exceeds the state of the art in computational capabilities due to $\underline{H}_F$ being a rank $N^3\times4$ complex matrix, where we desire N to be 100 or more because of the necessary balance between the lattice spacing and lattice length. For this reason, we compute the $1s$ state needed for calculating probabilities for K-shell capture of leptons by a partial eigensolution of $\underline{H}_F$.

Standard methods for partial eigensolution of large matrices which are designed to converge to the lowest-energy eigenstate of the spectrum are not directly applicable for computing the $1s$ state of $\underline{H}_F$ because of its

negative-energy continuum. In Ref. [15], the $1s$ state was computed using the damped-relaxation method [28]. In this method, the ground-state solution is determined by repeated application of a damping operator to a trial vector which removes the high-frequency components from the residual. The damping method does not depend on the spectrum being positive definite. As we wish to perform calculations with larger lattice sizes, we now use the more efficient iterative Lanczos algorithm [29,30] to compute the $1s$ state. The Lanczos algorithm has features which are attractive for our purposes; the memory requirements are relatively small and the method approximates external eigenvalues in the spectrum very well. However, the algorithm is limited in that it cannot distinguish eigenvectors of degenerate eigenvalues, i.e., the solutions are not eigenstates of the projection of the total angular momentum as noted in Sec. II B. Since the Lanczos algorithm converges most rapidly for extremal eigenvalues, we apply the Lanczos algorithm to $\underline{H}_F^2$, which has a positive-definite spectrum, and solve for the lowest energy eigenstate of $\underline{H}_F^2$. Thus, in solving for the ground state of $\underline{H}_F^2$, we obtain the lowest-energy bound state of $\underline{H}_F$. A description of the numerical details of our implementation of both the damped relaxation and the Lanczos algorithms can be found elsewhere [31].

We approximate the continuum states of $\underline{H}_F$ by modifying the eigenstates of the lattice representation of the free Dirac Hamiltonian $H_0=-i\boldsymbol{\alpha}\cdot\boldsymbol{\nabla}+\beta$ to be orthogonal to the bound states of $\underline{H}_F$, i.e., $\underline{\chi}^{\mu_b}_{E_b,\kappa_b}$. Even though the free Dirac continuum states are known analytically, we cannot use these states in our lattice calculation by simply evaluating the continuous functions at the lattice points, as such states would not be eigenstates of our lattice Hamiltonian. To be consistent, we must construct the eigenstates of $\underline{H}_0$, which we denote as $\underline{\xi}_{a,\lambda,s}$, on the lattice

$$\underline{H}_0\underline{\xi}_{a,\lambda,s}=\lambda E_a\underline{\xi}_{a,\lambda,s};\quad \lambda=\pm 1\ , \tag{64}$$

where s is the helicity. This construct is described in Appendix A.

We construct approximate Furry continuum lattice states following the projection operator techniques described in Ref. [32]. We define the projection operator $\underline{P}$ as

$$\underline{P}\equiv\underline{1}-\sum_{b=1}^{n_b}\underline{\chi}^{\mu_b}_{E_b,\kappa_b}\underline{\chi}^{\dagger\mu_b}_{E_b,\kappa_b}\ , \tag{65}$$

and modified continuum states as

$$\underline{\bar{\chi}}_{a,\lambda,s}\equiv\underline{P}\,\underline{\xi}_{a,\lambda,s}\ , \tag{66}$$

where n_b is the number of bound states contained in the spectrum of $\underline{H}_F$. By construction, these modified continuum states are orthogonal to the exact Furry bound states

$$\underline{\bar{\chi}}^{\dagger}_{a,\lambda,s}\chi^{\mu_b}_{E_b,\kappa_b}=0\ . \tag{67}$$

Therefore we impose upon the free Dirac continuum the correct initial condition that transition S-matrix elements between bound and continuum states are zero before switching on the interaction [33]. Currently, the sum in Eq. (65) includes only the $1s$ bound state. Other methods exist for constructing the Furry-continuum states on the lattice which are numerically more difficult [34].

D. Time evolution

The formal solution of the time-dependent Dirac equation Eq. (14) is

$$\psi_j(t)=\hat{U}(t,t_0)\psi_j(t_0)\ , \tag{68}$$

where we have omitted the spatial coordinates for simplicity and the time propagator $\hat{U}(t,t_0)$ is given, as shown in Eq. (19), by

$$\hat{U}(t,t_0)=\mathcal{T}\exp\left[-i\int_{t_0}^{t}dt'[H_F+H_P(t')]\right]\ . \tag{69}$$

In practical calculations, we begin and end time evolution at large, finite times $\pm T$. We discretize time in the sense that the electromagnetic interactions are taken as constant in successive small intervals of potentially varying size Δt_l,

$$t_l=\sum_{n=1}^{l}\Delta t_n\ ,\quad l=0,1,2,\ldots,L \tag{70}$$

and express the evolution operator in successive infinitesimal factors

$$\hat{U}(t,t_0)=\hat{U}(t,t_{L-1})\hat{U}(t_{L-1},t_{L-2}),\ldots,\hat{U}(t_1,t_0)\ . \tag{71}$$

In this case the time-ordering operator $\mathcal{T}$ can be ignored.

A number of different methods have been employed in the approximation of the infinitesimal time-evolution operator

$$\hat{U}(t_{l+1},t_l)=\exp\{-i[H_F+H_P(t_{l+1})]\Delta t_{l+1}\}\ , \tag{72}$$

particularly in studies of the time-dependent Hartree-Fock method applied to atomic and nuclear collisions [35,36]. The choice of a method usually depends on the dimensionality and structure of the Hamiltonian matrix. Several methods that work well in one- and two-dimensional problems are inapplicable for unrestricted three-dimensional problems because they require the inversion of part or all of the Hamiltonian matrix [35]. In our three-dimensional solution of the Dirac equation, the exponential operator, Eq. (72), is implemented as a Taylor-series expansion

$$\underline{\hat{U}}(t_{l+1},t_l)\approx\left[1+\sum_{k=1}^{K}\frac{(-i\Delta t_{l+1}[\underline{H}_F+\underline{H}_P(t_{l+1})])^k}{k!}\right], \tag{73}$$

where K is the maximum number of terms allowed in the Taylor-series expansion.

In summary, all of the numerical procedures discussed for implementing our lattice methods reduce to a series of (matrix)$\times$(vector) operations which can be executed with high efficiency on vector or parallel supercomputers without explicitly storing the matrix in memory. We implement our numerical methods on the CRAY-2 supercomputers at the National Center for Supercomputing

Applications in Illinois and the National Energy Research Supercomputer Center at Lawrence Livermore National Laboratory. Also, a version of our code has been adapted to the parallel architecture of the Intel i860/RX hypercube at the Oak Ridge National Laboratory. The Intel i860/RX is a distributed-memory, multiple-instruction, multiple-data supercomputer with 128 processors and 8 Mbytes of memory per processor. The peak speed of each processor is rated at 60 Mflops in double precision leading to the aggregate speed of 7.6 Gflops. As with most parallel implementations, we face the problems of limited memory per processor and the optimization of the algorithm to minimize communication between processors. The description of our solution to these problems can be found elsewhere [31].

IV. ELECTROMAGNETIC INTERACTION

In Sec. II, we saw that the physics of lepton-pair production is defined by the electromagnetic fields of two particles in relative motion, and that these fields enter the Hamiltonian via the dimensionless interaction energy $\overline{A}^{\mu}\equiv -eA^{\mu}$ between the lepton and the colliding nuclei in Eqs. (10) and (11). We assume a spherical and homogeneous charge density for both the projectile and the target, as finite-nuclear-size effects are important in the $1s$ state for heavy leptons. Therefore the static Coulomb interaction between the target nucleus and the lepton is

$$\overline{A}^{0}_{T}(r)=-(Z_T\alpha)f(r,R_T)\ , \tag{74}$$

where Z_T and R_T denote the charge number and root-mean-square charge radius of the target nucleus, respectively, and

$$f(r,R)=\begin{cases}\dfrac{1}{r}\ , & r>R\\ \dfrac{1}{2R}\left[3-\dfrac{r^2}{R^2}\right], & r\le R\ .\end{cases} \tag{75}$$

The time-dependent interaction, Eq. (11), arises because of the classical motion of the projectile. We neglect recoil effects. Therefore the projectile moves with constant velocity β_f along a straight-line trajectory, with impact parameter b, in the fixed-target frame of reference. We choose the projectile to move in the z direction and the reaction plane to be the y-z plane, i.e., the classical trajectory of the projectile is $x_P(t)=0, y_P(t)=b, z_P(t)=\beta_f t$.

A. Lorentz gauge

Since the Dirac equation is covariant under a gauge transformation of the electromagnetic potentials, the gauge may be chosen for convenience in any problem. The most familiar gauge used in problems with electric sources is the Lorentz gauge, defined by the condition $\partial_{\mu}A^{\mu}=0$. Since we assume a straight-line, constant velocity trajectory for the projectile motion, the time-dependent electromagnetic interaction between the projectile and the lepton in the Lorentz gauge can be generated by a Lorentz boost of the static Coulomb field, Eq. (74). This results in

$$\begin{aligned}&\overline{A}^{0}_{P}(r'(t))=-Z_P\alpha\gamma_f f(r'(t),R_P)\ ,\\ &\overline{A}^{3}_{P}(r'(t))=\beta_f\overline{A}^{0}_{P}(r'(t))\ ,\\ &\overline{A}^{1}_{P}=\overline{A}^{2}_{P}=0\ ,\end{aligned} \tag{76}$$

where Z_P and R_P are the atomic number and root-mean-square charge radius of the projectile, respectively. The Lorentz factor in the fixed-target frame is γ_f. The quantity $r'(t)$ is the distance between the lepton and the center of mass of the moving projectile in the target frame

$$r'(t)=[\rho'^2+\zeta^2(t)]^{1/2}\ , \tag{77}$$

where

$$\rho'\equiv[x^2+(y-b)^2]^{1/2}\ ,\quad \zeta(t)\equiv\gamma_f(z-\beta_f t)\ . \tag{78}$$

The beam energy for a given frame of reference is $E_{\rm kin}=m_0c^2(\gamma-1)$, where γ denotes the Lorentz factor for the frame of interest. The Lorentz factors for the fixed target and collider frames are related by $\gamma_f=2\gamma_c^2-1$. Figure 5 shows the temporal component of the muon's interaction energy with the target and projectile in the Lorentz gauge $\overline{A}^{0}(r'(t))=\overline{A}^{0}_{T}(r)+\overline{A}^{0}_{P}(r'(t))$ in a collision of ^{197}Au+^{197}Au at the collider energy of 100 GeV per nucleon.

Certain features of the interaction in the Lorentz gauge causes difficulties for our numerical methods. First, the interaction is very large as it is proportional to γ_f and

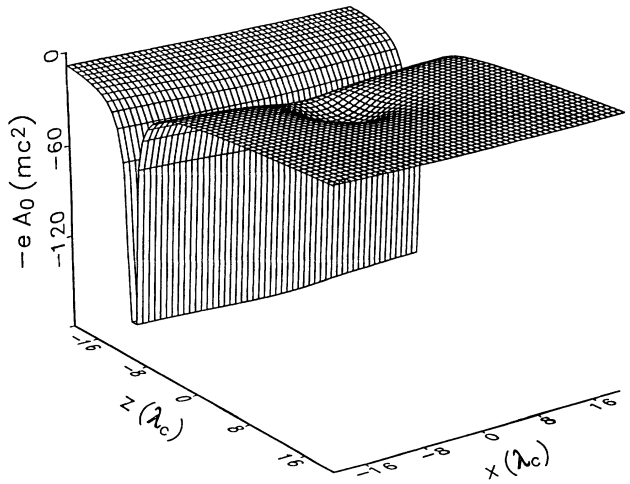

FIG. 5. Depicted is a slice taken at $y=0$ of the temporal component of the muon's interaction energy with a finite target and projectile in the Lorentz gauge $\overline{A}^{0}(r'(t))=\overline{A}^{0}_{T}(r)+\overline{A}^{0}_{P}(r'(t))$, in a collision of ^{197}Au+^{197}Au at a collider energy of 100 GeV per nucleon. The projectile nucleus, which is moving in the positive z direction, is presently centered at the point $(0,b_{\rm graz},-10\lambda_c)$, where $b_{\rm graz}=8.72\lambda_C$ is the grazing impact parameter. The static target is located at the origin. A square mesh with 51×51 points is used to represent the interaction. The narrow spike of the time-dependent interaction in this gauge is not well represented by this lattice spacing. Actually, the extremum of this interaction is $-1.41\times10^5 m_0c^2$.

sharply peaked in the boost direction e_3. Its width is proportional to γ_f^{-1} as a result of Lorentz contraction. Also, the long-range nature of the Coulomb potential is evident after the boost since the asymptotic dependence of the Lorentz gauge interaction is $|z-\beta_f t|^{-1}$. The large magnitude of the interaction requires that the time step be kept small so as to ensure a proper expansion of the time-evolution operator, Eq. (73). The long-range dependence of the interaction requires that we start numerical calculation at large distances between projectile and target to avoid switching on the interaction when its magnitude is appreciable. Another major difficulty lies in representing spiked functions with a finite lattice spacing. These features combine to make realistic, three-dimensional calculations of lepton-pair production too demanding computationally without some ameliorating methodology [15].

B. Axial gauge

Another gauge choice exists which, for relativistic energies, produces an interaction better represented on the lattice [37]. We are motivated towards our choice of gauge by the fact that the temporal component $\overline{A}_P^0(r'(t))$ and the component of the vector interaction in the boost direction $\overline{A}_P^3(r'(t))$ are proportional in the Lorentz gauge with proportionality constant β_f. Therefore important numerical cancellations occur between the vector and scalar components of the interaction in the projectile Hamiltonian H_P [38]. We attempt to remove the problematic behavior of the Lorentz gauge interaction on the lattice by performing a gauge transformation with a gauge function Λ designed such that the z component of the interaction in the new gauge is required to be zero, i.e.,

$$\overline{A}_P^3(r'(t))\rightarrow \tilde{A}_P^3(r'(t))=\overline{A}_P^3(r'(t))+\partial_z\Lambda(r'(t))\equiv 0 \ . \tag{79}$$

Therefore the definition of the axial-gauge function is

$$\Lambda(r'(t);z_0)\equiv -\beta_f\int_{z_0}^{z}\overline{A}_P^0(r'(t))dz \ , \tag{80}$$

where z_0 is an arbitrary integration constant. The parameter z_0 will affect the form of the interaction, but has no physical significance. We discuss the details of the axial-gauge interaction for a finite-size projectile in Appendix B. The important features of the transformation are illustrated here by considering the pointlike projectile, i.e., $R_P=0$. In this case, the gauge function Λ has the simple form

$$\Lambda(r'(t);z_0)=Z\alpha\beta_f\ln\frac{\zeta(t)+[\zeta^2(t)+\rho'^2]^{1/2}}{\zeta_0(t)+[\zeta_0^2(t)+\rho'^2]^{1/2}} \ , \tag{81}$$

where $\zeta_0(t)\equiv\gamma_f(z_0-\beta_f t)$. The gauge constant z_0 is restricted to be finite as

$$\lim_{z_0\rightarrow\pm\infty}\Lambda(r'(t);z_0)\rightarrow\mp\infty \ . \tag{82}$$

With such a finite choice for z_0, the axial-gauge transformation has no analytical effect on the static Furry states of the system, which are the asymptotic in and out states of the problem, as

$$\lim_{t\rightarrow\pm\infty}\Lambda(r'(t);z_0)\rightarrow 0 \ . \tag{83}$$

However, in our numerical calculations, z_0 should be chosen within the range $-\beta_f T<z_0<+\beta_f T$ for the limit in Eq. (83) to be reached in practical terms.

The lepton's interaction with the projectile in the axial gauge is found by using $\Lambda(r'(t);z_0)$ in a gauge transformation,

$$\overline{A}_p^\mu(r'(t))\rightarrow\tilde{A}_P^\mu(r'(t);z_0)=\overline{A}_P^\mu(r'(t))-\partial^\mu\Lambda(r'(t);z_0) \ . \tag{84}$$

The temporal, x, and y components of the lepton's interaction with a point-like projectile are

$$\tilde{A}_P^0(r'(t);z_0)=\frac{1}{\gamma_f^2}\overline{A}_P^0(r'(t))+\beta_f^2\overline{A}_P^0(r'(t))_{z=z_0} \ , \tag{85}$$

$$\tilde{A}_P^1(r'(t);z_0)=-Z_\alpha\beta_f\frac{x}{\rho'^2}\mathcal{Z}(r'(t);z_0) \ , \tag{86}$$

$$\tilde{A}_P^2(r'(t);z_0)=-Z\alpha\beta_f\frac{y-b}{\rho'^2}\mathcal{Z}(r'(t);z_0) \ , \tag{87}$$

where the time and z dependence of the x and y components of the interaction are contained in the factor

$$\mathcal{Z}(r'(t);z_0)\equiv\left[\frac{\zeta(t)}{[\zeta^2(t)+\rho'^2]^{1/2}}-\frac{\zeta_0(t)}{[\zeta_0^2(t)+\rho'^2]^{1/2}}\right] . \tag{88}$$

Notice that in the limit $\beta_f\rightarrow 0$, Eqs. (85)–(87) return to the static Coulomb interaction; in fact,

$$\lim_{\beta_f\rightarrow 0}\Lambda(r'(t);z_0)=0 \ . \tag{89}$$

By observing each component of the axial-gauge interaction, we notice that the problematic behavior of the lattice implementation of the Lorentz-gauge interaction in the high-energy limit is removed and replaced with structures which work well with our numerical methods. The temporal component's first term is proportional to γ_f^{-1} and, therefore, is negligible in the high-energy limit. Its second term is a broad function, since it is independent of z, and has a long-range $|z_0-\beta_f t|^{-1}$ dependence. In the limit $\zeta(t)\gg\rho'$ (i.e., $z\neq\beta_f t$ with high energies and moderate impact parameters), the z-dependent factor in the x and y components of the axial-gauge interaction has the simple form

$$\mathcal{Z}(r'(t);z_0)\approx\{\mathrm{sgn}[\zeta(t)]-\mathrm{sgn}[\zeta_0(t)]\} \tag{90}$$

to order γ_f^{-1}. Since z_0 is constrained to be inside the range of the projectile during the numerical calculation, the function $\mathcal{Z}(r'(t);z_0)$ is initially zero. It switches on to a value of 2 when $z_P(t)$ equals the minimum of z and z_0, and turns off when $z_P(t)$ equals the maximum of z and z_0. Therefore the axial-gauge interaction of a pointlike projectile in the limit $\zeta(t)\gg\rho'$ is

$$\tilde{A}_P^0(r'(t);z_0)\approx\frac{-Z_P\alpha\beta_f^2}{|z_0-\beta_f t|} \ , \tag{91}$$

$$\tilde{A}_P^1(r'(t);z_0)\approx -Z_P\alpha\beta_f\frac{x}{x^2+(y-b)^2}[\mathrm{sgn}(\zeta)-\mathrm{sgn}(\zeta_0)]\ , \tag{92}$$

$$\tilde{A}_P^2(r'(t);z_0)\approx -Z_P\alpha\beta_f\frac{y-b}{x^2+(y-b)^2}[\mathrm{sgn}(\zeta)-\mathrm{sgn}(\zeta_0)] \tag{93}$$

to order γ_f^{-1}. The divergence of the axial-gauge interaction for a pointlike projectile occurring along the trajectory of the projectile is removed by including finite-size effects. We emphasize that Eqs. (92) and (93) apply to a pointlike projectile and are presented here for illustration. We use the formulas presented in Appendix B for finite projectiles in the calculations performed for this paper.

In summary, the axial-gauge transformation removes the numerical difficulty associated with the spiked behavior of the Lorentz-gauge interaction, as $\tilde{A}_P^3(r'(t);z_0)=0$, and $\tilde{A}_P^0(r'(t);z_0)$ is a broad function independent of z. The switching on and switching off of the x and y components of the axial-gauge interaction does not demand extremely small lattice spacings, which are necessary when using the Lorentz gauge, to enable a faithful representation of the interaction on the lattice. Also, the numerical difficulties associated with the large magnitude and the long-range behavior of the Lorentz-gauge interaction have been greatly eased in the axial gauge. We see in Eqs. (92) and (93) that the x and y components of the axial-gauge interaction in the large γ_f limit [i.e., $\zeta(t)\gg\rho'$] are independent of γ_f to order γ_f^{-1}, and the extrema of these components of the interaction are on the same order of magnitude as the minimum of the target interaction $\tilde{A}_T^0$. These components are also clearly short ranged and allow the numerical calculation to begin with smaller distances between the projectile and the target. The scalar component of the axial-gauge interaction maintains the long-range nature of the Coulomb interaction; however, it is also independent of γ_f in the limit $\zeta(t)\gg\rho'$. Also, Eqs. (91)–(93) clearly show the leading impact-parameter dependence to be b^{-1}. Similar results have been obtained by a slightly different approach in Ref. [39]. Here the authors perform two consecutive gauge transformations in order to remove terms depending explicitly on γ_f or powers of b higher than b^{-1} in the high-energy limit of the multipole decomposition of the Lorentz-gauge interaction of the lepton with the projectile. Both of the gauge functions chosen in Ref. [39] show similarities to the axial-gauge function $\Lambda(r'(t);z_0)$. Figure 6 shows the x component of the axial-gauge interaction of the muon $\tilde{A}_P^1(r'(t);z_0)$ with a finite-sized projectile for the same 100 GeV per nucleon collider-frame collision shown in Fig. 5.

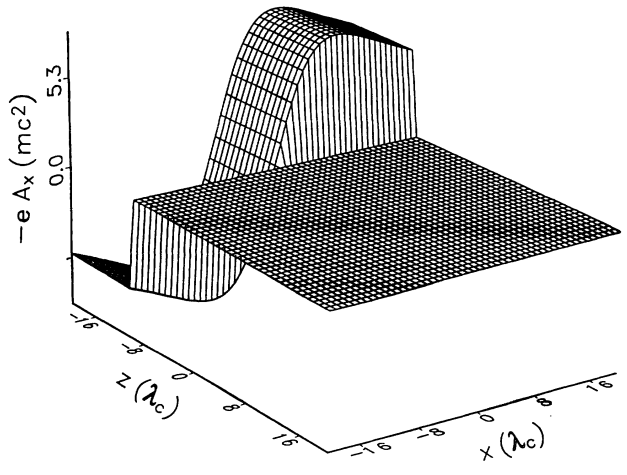

FIG. 6. Depicted is a slice taken at $y=0$ of the x component of the muon's time-dependent interaction energy with a finite-size projectile in the axial gauge $\tilde{A}_P^1(r'(t);z_0)$, in a 100 GeV per nucleon collision of ^{197}Au+^{197}Au in the collider frame with $z_0=100$. A square mesh with 51×51 points is used to represent the interaction. The projectile nucleus, which is moving in the positive z direction, is presently at the point $(0,b_{\mathrm{graz}},-10\lambda_C)$, where $b_{\mathrm{graz}}=8.72\lambda_C$ is the grazing impact parameter. Note the step-function behavior of the interaction.

V. RESULTS AND CONCLUSIONS

As stated earlier, we present here preliminary results for calculations of muon-pair production with capture of the negative muon into the K shell of the target atom. These results demonstrate the feasibility of solving nonperturbatively, in unrestricted three-dimensional coordinates, the lepton-capture problem for extremely relativistic energies using physical interactions. Our results are preliminary largely because of the small lattice sizes used in performing the calculations. Also, in this paper, we make no attempt to allow for long-range interactions between the projectile and the muon. That is, we do not allow for contributions to the capture probability from integrating Eq. (69) over times from $-\infty$ to $-T$ and $+T$ to $+\infty$.

The first step in computing this K-shell capture probability is the calculation of the $1s$ state of the Furry Hamiltonian. The static Coulomb interaction between the target nucleus and muon is evaluated for a homogeneous, spherical nuclear charge distribution with a radius $R=1.40A^{1/3}$ fm, where A is the atomic number. Using the basis-spline collocation method with fifth-order basis splines and the iterative Lanczos algorithm referred to in Sec. III, we compute the muonic $1s$ state of ^{197}Au on a lattice varying in number of points from 16 to 64 and with two lengths $L_1=L=40\lambda_c$ and $L_2=2L$ in the three Cartesian directions ($\lambda_C=1.87$ fm for muons). We require for the convergence of each solution that the energy fluctuation $\eta=[\langle H^2\rangle-\langle H\rangle^2]^{1/2}$ be less than 5.0×10^{-7}. For the lattice with 16 collocation points and length L_1 in each direction, the lattice spacing is $2.5\lambda_C$ and the Lanczos algorithm requires approximately 100 recursions to converge consuming 1 min of CRAY-2 CPU time. The number of recursions required for convergence depends more on the lattice spacing than on the number of lattice points, as we see by performing the static calculation using a lattice with 32 points and length L_2. The lattice spacing for this calculation is also $2.5\lambda_C$ and, as before, approximately 100 recursions are required for convergence. With the larger lattice length, the accuracy of

the energy improves by 0.3% and the CRAY-2 CPU time consumed increases to 5.3 min due to the larger vector lengths. Similarly, calculations with 32 points in a length L_1 and 64 points in a length L_2, each with lattice spacing $1.25\lambda_C$, require approximately 500 recursions to converge. The smaller and larger lattices consume 28 min and 4.5 h of CPU time, respectively. The energy eigenvalues obtained for a varying number of lattice points and sizes are shown in Fig. 7, where we fit the results obtained using the smaller box to the formula $E_{\rm fit}=0.911-5.16N^{-2}$, where N is the number of lattice points in each direction. The accuracy of our static solution is checked by performing an integration of the radial Dirac equations giving an energy of $E_R=0.9127m_0c^2$ for the muonic $1s$ state in ^{197}Au.

We perform the time development of the muonic $1s$ state of ^{197}Au, i.e., solve Eq. (14), on the lattice with 16 points and length L_1 in each direction under the influence of the time-dependent external fields produced in the collision of ^{197}Au+^{197}Au. A maximum number of 15 terms in the Taylor series expansion of the time-evolution operator is sufficient to preserve the norm of the time-dependent wave function to less than 1 part in 10^6 throughout the calculation. Four or five terms in the series are used on average. Conservation of the norm of the Dirac spinor is an important indicator for the numerical accuracy of the time development of the Dirac spinor.

We use the axial gauge for the interaction of the muon with the heavy ions. Initially, the projectile nucleus is positioned at $(0,b,-200\lambda_C)$, giving rise to a very small interaction with the muon at the position of the target nucleus which is fixed at the center of the cubic lattice. For collider energies less than 10 GeV per nucleon, we evolve the wave function for 2000 time steps with $\Delta t=0.2/\beta_f$ in units of $\tau_\mu=6.2\times10^{-24}$ s, stopping the evolution when the projectile is positioned at $(0,b,200\lambda_C)$. One such time-dependent run for a given impact parameter requires 33 min of CRAY-2 CPU time. For collider energies greater than 10 GeV per nucleon, we allow the size of the time step to vary in such a manner that Δt is inversely proportional to the maximum of the projectile's interaction with the muon. This ensures that the product $\Delta t_l[\underline{H}_F+\underline{H}_P(t_l)]$ in Eq. (73) remains less than one throughout the collision. Figure 8 shows the time dependence of the probability for capture into the $1s$ state of the muonic atom following pair creation from the vacuum for different choices of the axial-gauge parameter z_0. This figure numerically demonstrates the independence of the capture probabilities with respect to the gauge parameter.

We show the beam-energy dependence of the probability for K-shell muon capture in Fig. 9 by varying the energy per nucleon between 0.1 and 100 GeV in the collider frame of reference for the impact parameter $b=16.0\lambda_C$. Notice that the capture probability is independent of the beam energy for $E_c\geq 12$ GeV per nucleon. The energy independence of the interaction of the muon with the projectile in the high-energy limit was discussed in Sec. IV in the context of the axial gauge.

We show the impact-parameter dependence of the muon-capture probabilities at collider energies of 2 and 100 GeV per nucleon for a range of impact parameters in Fig. 10. For peripheral impact parameters (i.e., $b_{\rm graz}\leq b\leq b_{\rm cut}$), the capture probabilities have a power law impact-parameter dependence $P_{1s}(b)=Ab^{-Q}$, as shown by the fits to the results in Fig. 10, with $Q=3.7$ and 2.1 for the 2 and 100 GeV per nucleon collisions, re-

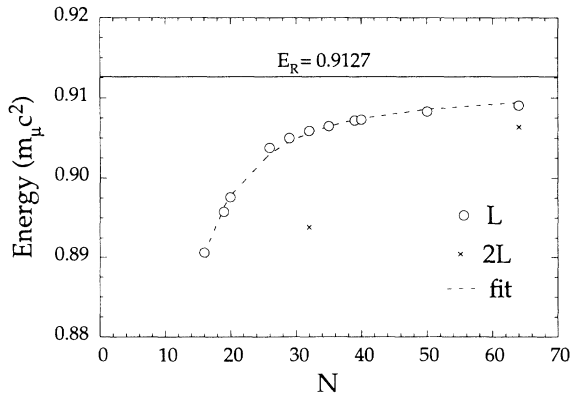

FIG. 7. Depicted are energies for the $1s$ muonic state of ^{197}Au computed with the basis-spline collocation method as a function of the number of lattice points N in each coordinate direction. The computations are performed for a lattice length $L=40\lambda_C$ and $2L=80\lambda_C$. The results for the smaller lattice length are fit to the formula $E_{\rm fit}=0.911-5.16N^{-2}$. The results for the larger lattice size are given to show that the accuracy of the computed energies improves as we increase the lattice length keeping the lattice spacing constant. We calculate the energy of this state to be $E_R=0.9127m_0c^2$ by integrating the radial Dirac equations.

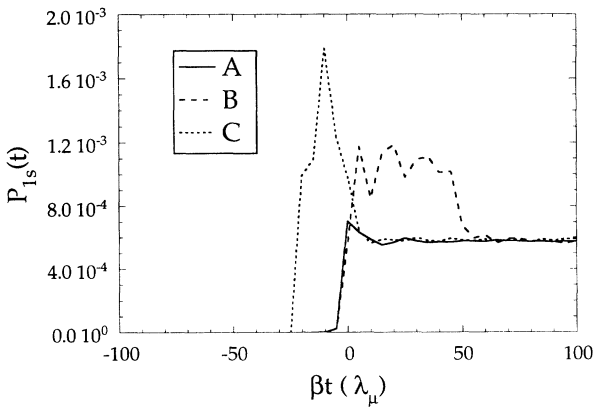

FIG. 8. Depicted are muon-capture probabilities into the $1s$ state as a function of the projectile velocity times the time (in units of $\lambda_C=1.87$ fm) for choices of the axial-gauge parameter of A, $z_0=0$; B, $z_0=+50$; and C, $z_0=-20$. The parameter z_0 defines a particular axial-gauge transformation and has no physical effect on the calculation. Muon pairs are produced electromagnetically from the QED vacuum in collisions of ^{197}Au+^{197}Au at a collider energy of 2.0 GeV per nucleon and impact parameter of $16.0\lambda_C$. The calculations are performed on a uniform cubic lattice with 16^3 points.

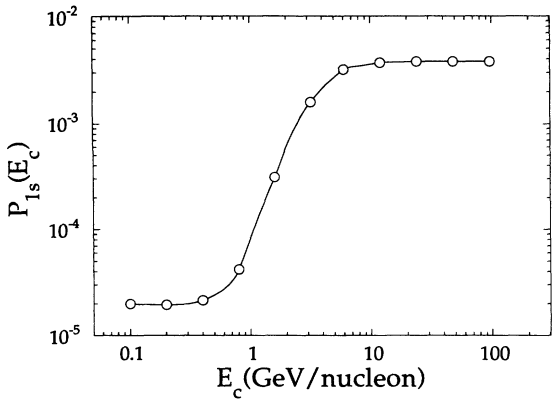

FIG. 9. Shown here are K-shell muon-capture probabilities in collisions of ^{197}Au+^{197}Au as a function of beam energy in the collider frame at the impact parameter $b=16.0\lambda_C$. The axial gauge is used for the electromagnetic interaction with $z_0=0$. The calculations are performed on a uniform cubic lattice with 16^3 collocation points. These results have yet to converge because of the use of the small lattice size.

spectively. The impact parameter $b_{\rm cut}$, is simply the largest impact parameter used for a given energy. The probabilities $P(b_{\rm cut})$ are on the same order of magnitude as the degree to which normalization of the time-dependent spinor is conserved. The grazing impact parameter is $b_{\rm graz}=8.72\lambda_C$ for ^{197}Au+^{197}Au collisions.

We calculate contributions to cross sections for muon capture into the K shell of ^{197}Au in peripheral collisions by integrating the capture probabilities in Fig. 10 over b, using the formula

$$\sigma_{1s}=2\pi\int_{b_{\rm graz}}^{\infty} bP_{1s}(b)db \ . \tag{94}$$

For $E_c=100$ GeV per nucleon, we do not integrate to infinity, but terminate the integration at $b=\gamma_f=2\times10^4\lambda_C$, which is a natural cutoff for the b

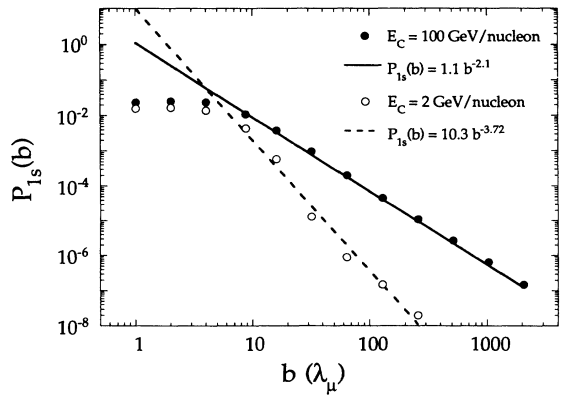

FIG. 10. Depicted are probabilities for muon capture into the K shell as a function of the impact parameter in units of λ_C for ^{197}Au+^{197}Au collisions at collider energies per nucleon of 2 and 100 GeV. The axial gauge is used for the electromagnetic interaction with $z_0=0$. We show power-law fits to the capture probabilities for impact parameters greater than grazing.

dependence of the probability. Therefore our preliminary estimates of the cross section for muon-pair production with K-shell capture in peripheral collisions of ^{197}Au+^{197}Au are 0.033 and 1.05 b for collider energy per nucleon of 2 and 100 GeV, respectively. We stress that our nonperturbative calculations have not converged largely due the small size of our lattice.

ACKNOWLEDGMENTS

This research was sponsored in part by the U.S. Department of Energy under Contract No. DE-AC05-84OR21400 with Martin Marietta Energy Systems, Inc. and under Contract No. DE-FG05-87ER40376 with Vanderbilt University. The numerical calculations were carried out on the CRAY-2 supercomputers at the National Center for Supercomputing Applications, in Illinois, and the National Energy Research Supercomputing Center at Lawrence Livermore National Laboratory, and the Intel iPSC/860 hypercube multicomputer at the Oak Ridge National Laboratory. One of the authors (J.C.W.) would like to acknowledge useful conversations with Dr. M. J. Rhoades-Brown.

APPENDIX A: EIGENSOLUTION OF LATTICE-FREE DIRAC HAMILTONIAN

Following the example of Eq. (49), our lattice representation of the free Dirac Hamiltonian is the 4×4 supermatrix

$$\underline{H}_0=-i\boldsymbol{\alpha}\cdot\underline{\mathbf{D}}+\beta \ . \tag{A1}$$

We proceed to construct the eigenstates of $\underline{H}_0$

$$\underline{H}_0\underline{\xi}_{a,\lambda,s}=\lambda E_a\underline{\xi}_{a,\lambda,s} \ , \quad \lambda=\pm1 \ , \tag{A2}$$

where s is the helicity quantum number, by first constructing the eigenstates of the lattice representation of the Foldy-Wouthuysen (FW) transformed Hamiltonian [19]

$$\underline{H}_0^{(\rm FW)}=\underline{F}\,\underline{H}_0\underline{F}^{\dagger}=\beta\sqrt{2\underline{T}+1} \ , \tag{A3}$$

where

$$\underline{F}=\frac{\beta\underline{H}_0+E_a}{\sqrt{2E_a(E_a+1)}} \ . \tag{A4}$$

As a result of the simple form of $\underline{H}_0^{(\rm FW)}$, only the lattice representation of the kinetic-energy operator $\underline{T}$ needs to be diagonalized, which is a manageable procedure. Using Eq. (62),

$$\underline{T}=\sum_{i=1}^{3}\underline{T}_i=-\tfrac{1}{2}\sum_{i=1}^{3}\underline{\Delta}_i \ . \tag{A5}$$

We diagonalize $\underline{T}_i$, giving all eigenvalues τ_{a_i} with associated orthonormal eigenvectors $\underline{\varphi}_{a_i}$

$$\underline{T}_i\underline{\varphi}_{a_i}=\tau_{a_i}\underline{\varphi}_{a_i}, \quad a_i=1,\ldots,N_i \ . \tag{A6}$$

Given the separability of the kinetic energy in Cartesian coordinates, the eigenvectors of $\underline{T}$ are products of the eigenvectors of $\underline{T}_i$,

$$\underline{T}\,\underline{\varphi}_a=\sum_{i=1}^{3}\underline{T}_i\underline{\varphi}_{a_1}\underline{\varphi}_{a_2}\underline{\varphi}_{a_3}=\tau_a\underline{\varphi}_a\ , \tag{A7}$$

with associated eigenvalues $\tau_a=(\tau_{a_1}+\tau_{a_2}+\tau_{a_3})$, where $a=1,\ldots,N_1N_2N_3$. Therefore, the eigenstates of $\underline{H}_0^{(\mathrm{FW})}$, denoted $\underline{\varphi}_{a,\lambda,s}$, are the product states of $\underline{\varphi}_a$ and the eigenvectors of β,

$$\begin{aligned}&\underline{\varphi}_{a,1,s}=\underline{\varphi}_a\otimes u_s\ ,\quad s=1,2,\quad a=1,\ldots,N_1N_2N_3\ ,\\&\underline{\varphi}_{a,-1,s}=\underline{\varphi}_a\otimes v_s\ ,\quad s=1,2,\quad a=1,\ldots,N_1N_2N_3\ ,\end{aligned} \tag{A8}$$

where the eigenvectors of β are

$$\begin{aligned}u_1&=\begin{bmatrix}1\\0\\0\\0\end{bmatrix},\quad u_2=\begin{bmatrix}0\\1\\0\\0\end{bmatrix},\\ v_1&=\begin{bmatrix}0\\0\\1\\0\end{bmatrix},\quad v_2=\begin{bmatrix}0\\0\\0\\1\end{bmatrix}.\end{aligned} \tag{A9}$$

The spinors $\underline{\varphi}_{a\lambda s}$ form a complete and orthonormal basis and are helicity eigenstates.

We now construct the free Dirac continuum states on the lattice by applying the inverse Foldy-Wouthuysen transformation in Eq. (A4) to the states $\underline{\varphi}_{a\lambda s}$,

$$\underline{\xi}_{a\lambda s}=\underline{F}^{\dagger}\underline{\varphi}_{a\lambda s}=\frac{\underline{H}_0\beta+E_a}{\sqrt{2E_a(E_a+1)}}\underline{\varphi}_{a\lambda s}\ . \tag{A10}$$

The new eigenstates $\underline{\xi}_{a\lambda s}$ are by construction exact eigenstates of $\underline{H}_0$,

$$\begin{aligned}&\underline{H}_0\underline{\xi}_{a\lambda s}=\lambda E_a\underline{\xi}_{a\lambda s}\ ,\quad \lambda=\pm1\ ,\\&E_a=\sqrt{2\tau_a+1}\ .\end{aligned} \tag{A11}$$

Since the states $\underline{\varphi}_{a\lambda s}$ are eigenstates of β, we can rewrite Eq. (A10) as

$$\underline{\xi}_{a\lambda s}=\frac{1}{2}\left[\frac{2E_a}{E_a+1}\right]^{1/2}\left[1+\frac{\underline{H}_0}{\lambda E_a}\right]\underline{\varphi}_{a\lambda s}\ . \tag{A12}$$

APPENDIX B: AXIAL GAUGE WITH FINITE PROJECTILE

Here we present the axial-gauge transformation for the case of a spherical, finite-size, homogeneously charged projectile with radius R_P. As a result of performing the integral in Eq. (80), which defines the axial-gauge function, three different cases exist for the $\Lambda(r'(t);z_0)$ since z_0 is required to be finite by Eq. (82). If $z_0>\beta_f t+\gamma_f^{-1}(R_P^2-\rho'^2)^{1/2}$, then

$$\begin{aligned}\Lambda(r'(t);z_0)=Z\alpha\beta_f\Bigg[&\ln\frac{\zeta(t)+[\zeta^2(t)+\rho'^2]^{1/2}}{\zeta_0(t)+[\zeta_0^2(t)+\rho'^2]^{1/2}}\\&+\Theta(R_P-\rho')\Bigg\{\Theta((R^2-\rho'^2)^{1/2}-|\zeta(t)|)\\&\times\Bigg\{\ln\frac{R+(R^2-\rho'^2)^{1/2}}{\zeta(t)+[\zeta^2(t)+\rho'^2]^{1/2}}+\frac{1}{2}\left[3-\frac{\rho'^2}{R_P^2}\right]\left[\frac{\zeta(t)}{R_P}-\left[1-\frac{\rho'^2}{R_P^2}\right]^{1/2}\right]\\&\quad-\frac{\zeta^3(t)}{6R_P^3}+\frac{1}{6}\left[1-\frac{\rho'^2}{R_P^2}\right]^{1/3}\Bigg\}\\&+\Theta(-\zeta(t)-(R^2-\rho'^2)^{1/2})\Bigg[\ln\frac{R+(R^2-\rho'^2)^{1/2}}{R-(R^2-\rho'^2)^{1/2}}-\left[3-\frac{\rho'^2}{R_P^2}\right]\left[1-\frac{\rho'^2}{R_P^2}\right]^{1/2}\\&\quad+\frac{1}{3}\left[1-\frac{\rho'^2}{R_P^2}\right]\Bigg]\Bigg\}\Bigg]\ .\end{aligned} \tag{B1}$$

If $z_0<\beta_f t-\gamma_f^{-1}(R_P^2-\rho'^2)^{1/2}$, then

$$\begin{aligned}\Lambda(r'(t);z_0)=Z\alpha\beta_f\Bigg[&\ln\frac{\zeta(t)+[\zeta^2(t)+\rho'^2]^{1/2}}{\zeta_0(t)+[\zeta_0^2(t)+\rho'^2]^{1/2}}\\&+\Theta(R_P-\rho')\Bigg\{\Theta((R^2-\rho'^2)^{1/2}-|\zeta(t)|)\\&\times\Bigg\{\ln\frac{R-(R^2-\rho'^2)^{1/2}}{\zeta(t)+[\zeta^2(t)+\rho'^2]^{1/2}}+\frac{1}{2}\left[3-\frac{\rho'^2}{R_P^2}\right]\left[\frac{\zeta(t)}{R_P}+\left[1-\frac{\rho'^2}{R_P^2}\right]^{1/2}\right]\\&\quad-\frac{\zeta^3(t)}{6R_P^3}-\frac{1}{6}\left[1-\frac{\rho'^2}{R_P^2}\right]^{1/3}\Bigg\}\end{aligned}$$

$$+\Theta(\zeta(t)-(R^2-\rho'^2)^{1/2})\left[\ln\frac{R-(R^2-\rho'^2)^{1/2}}{R+(R^2-\rho'^2)^{1/2}}+\left[3-\frac{\rho'^2}{R_P^2}\right]\left[1-\frac{\rho'^2}{R_P^2}\right]^{1/2}-\frac{1}{3}\left[1-\frac{\rho'^2}{R_P^2}\right]^{1/3}\right]\right] . \tag{B2}$$

If $\gamma_f^{-1}(R_P^2-\rho'^2)^{1/2}\geq|z_0-\beta_f t|$, then

$$\begin{aligned}\Lambda(r'(t);z_0)=z\alpha\beta_f\Theta(R_P-\rho')&\left\{\frac{\zeta_0^3(t)}{6R_P^3}-\frac{\zeta_0(t)}{2R_P}\left[3-\frac{\rho'^2}{R_P^2}\right]\right.\\&+\Theta(\zeta(t)-(R^2-\rho'^2)^{1/2})\left[\ln\frac{\zeta(t)+[\zeta^2(t)+\rho'^2]^{1/2}}{R+(R^2-\rho'^2)^{1/2}}-\frac{1}{6}\left[1-\frac{\rho'^2}{R_P^2}\right]^{1/3}\right.\\&\left.\left.+\frac{1}{2}\left[1-\frac{\rho'^2}{R_P^2}\right]^{1/2}\left[3-\frac{\rho'^2}{R_P^2}\right]\right]\right.\\&+\Theta((R^2-\rho'^2)^{1/2}-|\zeta(t)|)\left[\frac{\zeta(t)}{2R_P}\left[3-\frac{\rho'^2}{R_P^2}\right]-\frac{\zeta^3(t)}{6R_P^3}\right]\\&+\Theta(-\zeta(t)-(R^2-\rho'^2)^{1/2})\left[\ln\frac{\zeta(t)+[\zeta^2(t)+\rho'^2]^{1/2}}{R-(R^2-\rho'^2)^{1/2}}+\frac{1}{6}\left[1-\frac{\rho'^2}{R_P^2}\right]^{1/3}\right.\\&\left.\left.-\frac{1}{2}\left[1-\frac{\rho'^2}{R_P^2}\right]^{1/2}\left[3-\frac{\rho'^2}{R_P^2}\right]\right]\right\} .\end{aligned} \tag{B3}$$

All factors in Eqs. (B1)–(B3) which contain the step function $\Theta(x)$ arise because of finite-size effects.

The interaction in the axial gauge is found by using each of Eqs. (B1)–(B3) in a gauge transformation

$$\overline{A}_P^\mu(r'(t))\rightarrow\tilde{A}_P^\mu(r'(t);z_0)=\overline{A}_P^\mu(r'(t))-\partial^\mu\Lambda(r'(t);z_0) . \tag{B4}$$

The results are the following. For the temporal component, the interaction is

$$\tilde{A}_P^0(r'(t);z_0)=\frac{1}{\gamma_f^2}\overline{A}_P^0(r'(t))+\beta_f^2\overline{A}_P^0(r'(t))_{z=z_0} . \tag{B5}$$

For the x and y components $\tilde{A}_P^1(r'(t);z_0)$ and $\tilde{A}_P^2(r'(t);z_0)$, there are again three cases for z_0. We list only the x component. The y component of the interaction may be obtained from the x component by multiplying by the factor $(y-b)/x$. For the case $z_0>\beta_f t+\gamma_f^{-1}(R_P^2-\rho'^2)^{1/2}$, the x component is

$$\begin{aligned}\tilde{A}_P^1(r'(t);z_0)=-Z\alpha\beta_f\frac{x}{\rho'^2}&\left\{\frac{\zeta(t)}{[\zeta^2(t)+\rho'^2]^{1/2}}-\frac{\zeta_0(t)}{[\zeta_0^2(t)+\rho'^2]^{1/2}}\right.\\&+\Theta((R_P^2-\rho'^2)^{1/2}-|\zeta(t)|)\left[\frac{\zeta(t)\rho'^2}{R_P^3}-\frac{\zeta(t)}{[\zeta^2(t)+\rho'^2]^{1/2}}+\left[1-\frac{\rho'^2}{R_P^2}\right]^{1/3}\right]\\&\left.+2\Theta(-\zeta(t)-(R_P^2-\rho'^2)^{1/2})\left[1-\frac{\rho'^2}{R_P^2}\right]^{1/3}\right\} .\end{aligned} \tag{B6}$$

For the case $|z_0-\beta_f t|\leq\gamma_f^{-1}(R_P^2-\rho'^2)^{1/2}$, if $|z-\beta_f t|\geq\gamma_f^{-1}(R_P^2-\rho'^2)^{1/2}$, the x component is

$$\begin{aligned}\tilde{A}_P^1(r'(t);z_0)=-Z\alpha\beta_f\frac{x}{\rho'^2}&\left[\frac{\zeta(t)}{[\zeta^2(t)+\rho'^2]^{1/2}}-\frac{\zeta_0(t)\rho'^2}{R_P^3}-\Theta(\zeta(t)-(R_P^2-\rho'^2)^{1/2})\left[1-\frac{\rho'^2}{R_P^2}\right]^{1/3}\right.\\&\left.+\Theta(-\zeta(t)-(R_P^2-\rho'^2)^{1/2})\left[1-\frac{\rho'^2}{R_P^2}\right]^{1/3}\right] ;\end{aligned} \tag{B7}$$

if $|z-\beta_f t|\leq\gamma_f^{-1}(R_P^2-\rho'^2)^{1/2}$, then the x component is

$$\tilde{A}_P^1(r'(t);z_0)=-Z_P\alpha\gamma_f\beta_f\frac{x}{R_P^3}(z-z_0) . \tag{B8}$$

For the case $z_0<\beta_f t-\gamma_f^{-1}(R_P^2-\rho'^2)^{1/2}$, the x component is

$$\tilde{A}_P^1(r'(t);z_0)=-Z\alpha\beta_f\frac{x}{\rho'^2}\left\{\frac{\zeta(t)}{[\zeta^2(t)+\rho'^2]^{1/2}}-\frac{\zeta_0(t)}{[\zeta_0^2(t)+\rho'^2]^{1/2}}\right.$$
$$+\Theta((R_P^2-\rho'^2)^{1/2}-|\zeta(t)|)\left[\frac{\zeta(t)\rho'^2}{R_P^3}-\frac{\zeta(t)}{[\zeta^2(t)+\rho'^2]^{1/2}}-\left[1-\frac{\rho'^2}{R_P^2}\right]^{1/3}\right]$$
$$\left.-2\Theta(\zeta(t)-(R_P^2-\rho'^2)^{1/2})\left[1-\frac{\rho'^2}{R_P^2}\right]^{1/3}\right\}. \tag{B9}$$

[1] C. Bottcher and M. R. Strayer, in Proceedings of the Second Workshop on Experiments and Detectors for RHIC, Berkeley, California, 1987, LBL Report No. LBL-24604, 1987 (unpublished).

[2] C. Bottcher and M. R. Strayer, Nucl. Instrum. Methods B **31**, 122 (1988).

[3] G. Baur, Brookhaven National Laboratory Workshop Proceedings, Upton, New York, BNL Report No. BNL-52247, 1990 (unpublished).

[4] C. Bottcher and M. Strayer, Phys. Rev. D **39**, 1330 (1989).

[5] M. Fatyga, M. J. Rhoades-Brown, and M. Tannenbaum, Brookhaven National Laboratory Workshop Proceedings, Upton, New York, BNL Report No. BNL-52247, 1990 (unpublished), p. 2.

[6] G. Domokos and J. Goldman, Phys. Rev. D **23**, 203 (1981); **28**, 123 (1983); K. Kajantie and H. I. Miettenen, Z. Phys. C. **9**, 341 (1981); Z. Phys. **14**, 357 (1982); K. Kajantie, M. Kataja, L. McLerran, and P. V. Ruuskanen, Phys. Rev. D **34**, 811 (1986); K. Kajantie, J. Kapusta, L. McLerran, and A. Mekjian, *ibid.* **34**, 2746 (1986).

[7] H. Gould, in *Atomic Theory Workshop on Relativistic and QED Effects in Heavy Atoms, Gaithersburg, 1985,* AIP Conf. Proc. No. 136, edited by Hugh P. Kelly and Yong-Ki Kim (AIP, New York, 1985).

[8] C. Bottcher and M. R. Strayer, in *Physics of Strong Fields,* Proceedings of the International Advanced Course, Maratea, Italy, 1986, Vol. 153 of *NATO Advanced Study Institute, Series B: Physics,* edited by W. Greiner (Plenum, New York, 1987), p. 629.

[9] E. Teller, in *Proceedings of the Ninth International Conference on the Application of Accelerators in Research and Industry,* edited by J. L. Duggan (North-Holland, New York, 1986).

[10] C. A. Bertulani and G. Baur, Phys. Rep. **163**, 299 (1988).

[11] J. Eichler, Phys. Rep. **193**, 167 (1990).

[12] W. Scheid, in (Ref. [3]); K. Momberger, N. Grün, and W. Scheid (unpublished); K. Rumrich, K. Momberger, G. Soff, W. Greiner, N. Grün, and W. Scheid, Phys. Rev. Lett. **66**, 2613 (1991).

[13] C. Bottcher and M. R. Strayer, Ann. Phys. (N.Y.) **175**, 64 (1987).

[14] A. S. Umar, J.-S. Wu, M. R. Strayer, and C. Bottcher, J. Comput. Phys. **93**, (1991).

[15] M. R. Strayer, C. Bottcher, V. E. Oberacker, and A. S. Umar, Phys. Rev. A **41**, 1399 (1990).

[16] J. Reinhardt, B. Müller, and W. Greiner, Phys. Rev. A **24**, 103 (1981).

[17] G. Soff, J. Reinhardt, B. Müller, and W. Greiner, Z. Phys. A **294**, (1980).

[18] J. F. Reading and A. L. Ford, Phys. Rev. A **21**, 24 (1980).

[19] C. Itzykson and J. B. Zuber, *Quantum Field Theory* (McGraw-Hill, New York, 1980).

[20] A. S. Davydov, *Quantum Mechanics,* 2nd ed. (Pergamon, Oxford, 1965); J. M. Jauch and F. Rohrlich, *The Theory of Photons and Electrons,* 2nd ed. (Springer-Verlag, New York, 1976), p. 140ff; F. Coester, Phys. Rev. **84**, 1259 (1951).

[21] T. A. Green, Proc. Phys. Soc. **86**, 1017 (1965); R. Shakeshaft, J. Phys. B **5**, 559 (1972); R. Shakeshaft and J. Macek, *ibid.* **5**, L63 (1972); R. Shakeshaft, J. Macek, and E. Gerjuoy, *ibid.* **6**, 794 (1973); J. F. Reading, Phys. Rev. A **8**, 3262 (1973).

[22] J. Rabin, Phys. Rev. D **24**, 3218 (1981).

[23] L. H. Karsten and J. Smit, Nucl. Phys. **B183**, 103 (1981).

[24] L. H. Kartsen, Phys. Lett. **104B**, 315 (1981).

[25] H. B. Nielsen and M. Ninomiya, Phys. Lett. **105B**, 219 (1981).

[26] J. Rabin, Nucl. Phys. **B201**, 315 (1982).

[27] R. Stacy, Phys. Rev. D **26**, 468 (1982).

[28] C. Bottcher, M. R. Strayer, A. S. Umar, and P.-G. Reinhard, Phys. Rev. A **40**, 4182 (1989).

[29] J. Cullum, R. Willoughby, *Lanczos Algorithms for Large Symmetric Eignevalue Compuatations, Vol. I* (Birkhäuser, Boston, 1985).

[30] B. Parlett, *The Symmetric Eigenvalue Problem* (Prentice-Hall, Englewood Cliffs, NJ, 1980).

[31] J. C. Wells, V. E. Oberacker, A. S. Umar, C. Bottcher, M. R. Strayer, J.-S. Wu, J. Drake, and R. Flanery (unpublished).

[32] H. Feshbach, Rev. Mod. Phys. **36**, 1076 (1964).

[33] R. R. Scheerbaum, C. M. Shakin, and R. M. Thaler, Ann. Phys. (N.Y.) **76**, 333 (1973).

[34] C. Bottcher, M. R. Strayer, A. S. Umar, and V. E. Oberacker, Phys. Rev. C **37**, 2487 (1988).

[35] A. S. Umar and M. R. Strayer, Comput. Phys. Commun. **63**, 179 (1991).

[36] C. Bottcher, G. J. Bottrell, and M. R. Strayer, Comput. Phys. Commun. **63**, 63 (1991).

[37] G. Katz, G. Batrouni, C. Davis, A. Kronfeld, P. Lepage, P. Rossi, B. Svetitsky, and K. Wilson, Phys. Rev. D **37**, 1589 (1988).

[38] P. A. Amundsen and K. Aashamar, J. Phys. B **14**, 4047 (1981).

[39] A. J. Baltz, M. J. Rhoades-Brown, and J. Weneser, Phys. Rev. A **44**, 5569 (1991).